TABLE 1—(*Continued*)

JCI No	Name	Abbreviation	Application/Target/Mechanism
−418	Acrylamide		Neurotoxin/carcinogenicity
−417	Hexachlorobenzene	BHC	Agricultural chemical/carcinogenicity
−346	2-Deoxyglucose	2-DG	Glycolytic pathway/glycosylation inhibitor
−325	Pentachlorophenol	PCP	Agricultural chemical/teratogenicity/carcinogenicity
−324	Aniline		Oxidative stress/methemoglobinemia/carcinogenicity
−323	Triazine		Agricultural chemical
−322	Edifenphos	EDDP	Agricultural chemical/antibiotics/choline esterase
−321	γ-1,2,3,4,5,6-Hexachlorocyclohexane	γ-BHC	Agricultural chemical/carcinogenicity
−320	Dichlorvos	DDVP	Agricultural chemical/teratogenicity/carcinogenicity
−319	*O*-Ethyl *O*-4-nitrophenyl phenylphosphonothioate	EPN	Agricultural chemical
−318	Cadmium chloride	$CdCl_2$	Teratogenicity/carcinogenicity
−317	Phenylmercury acetate	PMA	Fungicides/mutagenicity
−316	Mercaptoacetic acid		Synthetic intermediate
−315	1,3-Diphenylguanidine	DPG	Vulcanizing agent
−314	3,4,4′-Trichlorocarbanilide	TCC	Cosmetics/antibacterial agent
−313	3-Iodo-2-propynyl butylcarbamate	IPBC	Antibacterial agent
−311	2,3,3,3−2′,3′,3′,3′-Octachlorodipropylether	S-421	Agricultural chemical/antibacterial agent
−310	1,2-Benzisothiazolin-3-one	BIT	Antibacterial agent
−309	Isobornylthiocyanoacetate	IBTA	Antibacterial agent
−308	*p*-Chlorophenyl-3-iodopropargylformal	CPIP	Antibacterial agent
−307	Zinc butylxanthate	ZBX	Vulcanizing agent
−306	Polypropylene glycol	PG	Synthetic intermediate
−305	10,10′-Oxy-bis(phenoxyarsine)	OBPA	Antibacterial agent
−296	Snake venom from *Naja naja kaouthia*	SV-NNK	Snake venom
−295	Snake venom from *Naja nigricollis*	SV-NN	Snake venom
−294	2,5-di(*tert*-butyl)-1,4-Hydroquinone	DTBHQ	Oxidative stress
−293	Ibotenic Acid		Mushroom toxin/neurotoxin
−292	*N*-Methy-4-phenyl-1,2,3,6-tetrahydropyridine	MPTP	Neurotoxin
−289	Tetrodotoxin		Natural product/Na^+ channel inhibitor
−288	ICI 182,780		Estrogen antagonist
−275	Benzophenone		Agricultural chemical
−274	1,2-Dibromo-3-chloropropane	DBCP	Antibacterial agent/insecticide/carcinogenicity
−273	Zineb		Agricultural chemical
−272	Dieldrin		Insecticide
−271	Hexachlorobenzene	HCB	Antibacterial agent/carcinogenicity
−270	Ziram		Antibacterial agent/vulcanizing agent
−269	Chlordane		Insecticide/carcinogenicity
−268	4,4′-Dichlorodiphenyltrichloroethane	p,p′-DDT	Insecticide/carcinogenicity/teratogenicity
−267	Bisphenol A	BPA	Estrogenic
−266	17-β-Estradiol	E2	Estrogenic
−265	Diethylstilbestrol	DES	Estrogenic
−261	Paraquat		Agricultural chemical/oxidative stress
−247	Ouabain		Cardiac glycosides
−245	Okadaic acid		Natural product/PP1, PP2A inhibitor
−242	Antimycin A1		Agricultural chemical
−232	Digoxin		Cardiac glycosides
−201	OH-Flutamide		Flutamide derivative/androgen antagonist
−200	Flutamide		Anticancer drugs/androgen antagonist
−185	30% H_2O_2		Oxidative stress
−182	*N*-Acetyl-L-cysteine	NAC	Super oxyside scavenger
−181	L-Ascorbic acid		Food constituent
−179	Dopamine		Neurotransmitter
−177	Caffeine		Food constituent
−168	Cycloheximide		Protein synthesis inhibitor
−144	4-Hydroxyphenylretinamide	4-HPR	RAR
−137	Indomethacin		COX inhibitor
−99	SN-38		Irinotecan derivative/Topo I
−96	Toremifene		Anticancer drugs/estrogen antagonist
−95	Tamoxifen		Anticancer drugs/estrogen antagonist
−63	Cyclosporin A		Anticancer drugs/helper T cell
−46	HCFU		Anticancer drugs/antimetabolite(pyrimidine)
−36	Docetaxel		Anticancer drugs/tubulin
−35	Paclitaxel		Anticancer drugs/tubulin
−34	Colchicine		Antipodagric/tubulin
−33	Cisplatin		Anticancer drugs/DNA cross linker
−32	Carboplatin		Anticancer drugs/DNA cross linker
−31	Irinotecan		Anticancer drugs/Topo I
−30	Camptothecin	CPT	Anticancer drugs/Topo I
−24	Methotrexate		Anticancer drugs/DHFR
−19	Vincristine		Anticancer drugs/tubulin
−18	Vinblastine		Anticancer drugs/tubulin
−16	Mitomycin-C	MMC	Anticancer drugs/DNA alkylator
−9	Tegafur		Anticancer drugs/antimetabolite(pyrimidine)
−8	5-Fluorouracil	5-FU	Anticancer drugs/antimetabolite(pyrimidine)
−5	Cytarabine		Anticancer drugs/antimetabolite(pyrimidine)
−4	Nitrogen mustard		Anticancer drugs/DNA alkylator

RAR, retinoic acid receptor; RXR; retinoid X receptor.

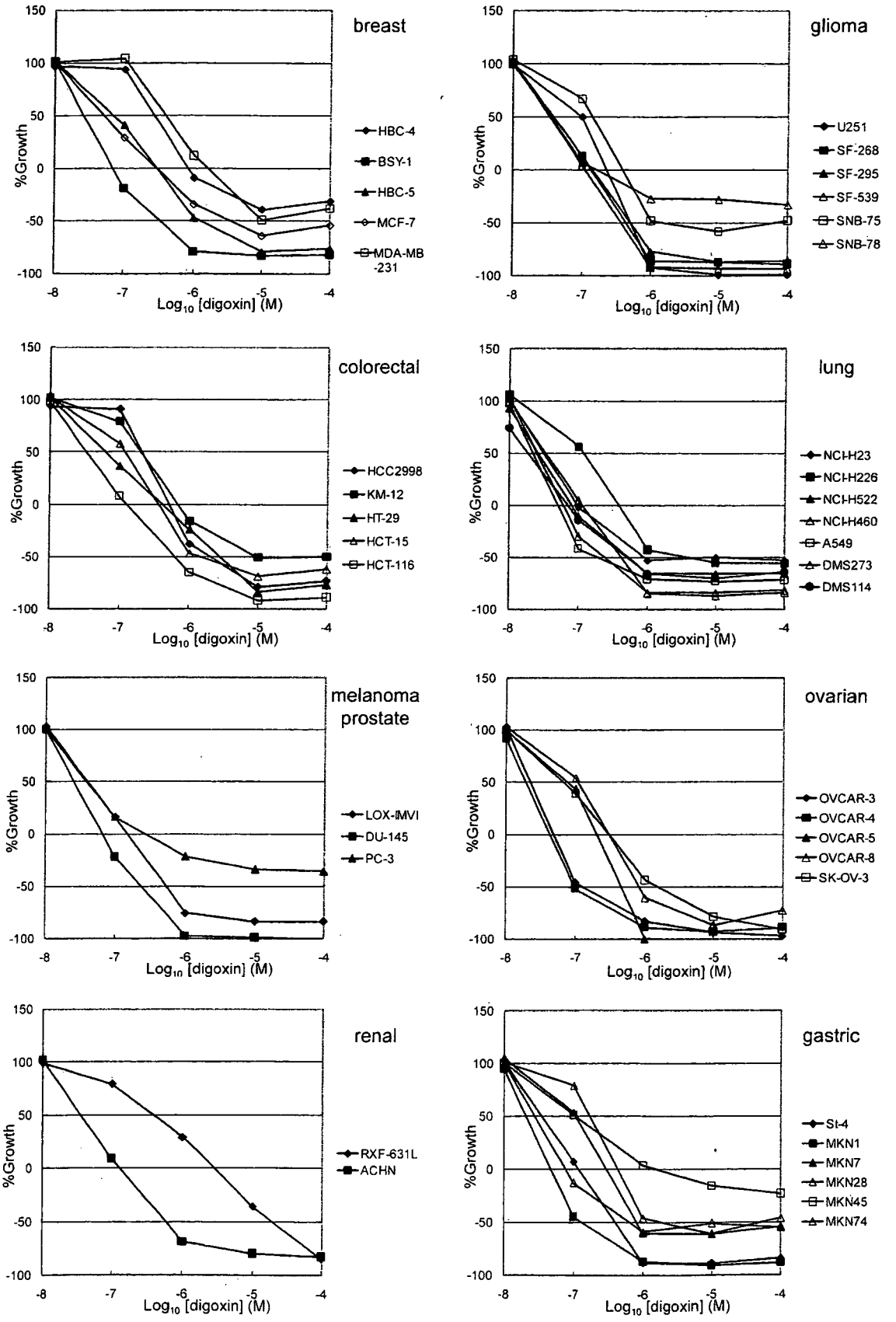

Fig. 1. Dose response curves of digoxin against growth of JFCR-39 cells. The *x*-axis represents concentration of digoxin and the *y-axis* represents percentage growth. The GI50 represents the concentration required to inhibit cell growth by 50% compared with untreated controls.

the standard anticancer drugs using the COMPARE algorithm (Yamori et al., 1999). We have used this system successfully and demonstrated that the molecular targets of the novel chemicals MS-274, FJ5002, and ZSTK474 were topoisomerases I and II (Yamori et al., 1999), telomerase (Naasani et al., 1999), and phosphatidylinositol 3-kinase (Yaguchi et al., 2006), respectively. Several other interesting studies, based on a panel of cancer cells, classified anticancer drugs according to their action mechanisms or molecular targets by cluster analysis of their GI50 values (Weinstein et al., 1992, 1997; Dan et al., 2002). Correlation analysis has also been used to explore the genes associated with the sensitivity of the cells in the panel to anticancer drugs (Scherf et al., 2000; Okutsu et al., 2002; Zembutsu et al., 2002; Nakatsu et al., 2005).

In this study, we have examined the potential of the JFCR39 system in classifying various chemicals, and predicted their action mechanisms. For this purpose, we have determined the fingerprints of 130 different types of chemicals including toxic chemicals, pesticides, drugs and synthetic intermediates, and then classified these chemicals according to the cluster analysis of their fingerprints.

Materials and Methods

Cell Lines and Cell Cultures. The panel of human cancer cell lines has been described previously (Yamori et al., 1999; Dan et al., 2002) and consists of the following 39 human cancer cell lines: lung cancer, NCI-H23, NCI-H226, NCI-H522, NCI-H460, A549, DMS273, and DMS114; colorectal cancer, HCC-2998, KM-12, HT-29, HCT-15, and HCT-116; gastric cancer, MKN-1, MKN-7, MKN-28, MKN-45, MKN-74, and St-4; ovarian cancer, OVCAR-3, OVCAR-4, OVCAR-5, OVCAR-8, and SK-OV-3; breast cancer, BSY-1, HBC-4, HBC-5, MDA-MB-231, and MCF-7; renal cancer, RXF-631L and ACHN; melanoma, LOX-IMVI; glioma, U251, SF-295, SF-539, SF-268, SNB-75, and SNB-78; and prostate cancer, DU-145 and PC-3. All cell lines were cultured in RPMI 1640 medium (Nissui Pharmaceutical, Tokyo, Japan) with 5% fetal bovine serum, penicillin (100 units/ml), and streptomycin (100 μg/ml) at 37°C under 5% CO_2.

Determination of Cell Growth Inhibition Profiles. Growth inhibition experiments were performed to assess the sensitivity of the cells to various chemicals as described before (Yamori et al., 1999; Dan et al., 2002). Growth inhibition was measured by determining the changes in the amounts of total cellular protein after 48 h of chemical treatment using a sulforhodamine B assay. For each chemical, the growth assay was performed using a total of five different concentrations of the chemical (for example, 10^{-4}, 10^{-5},

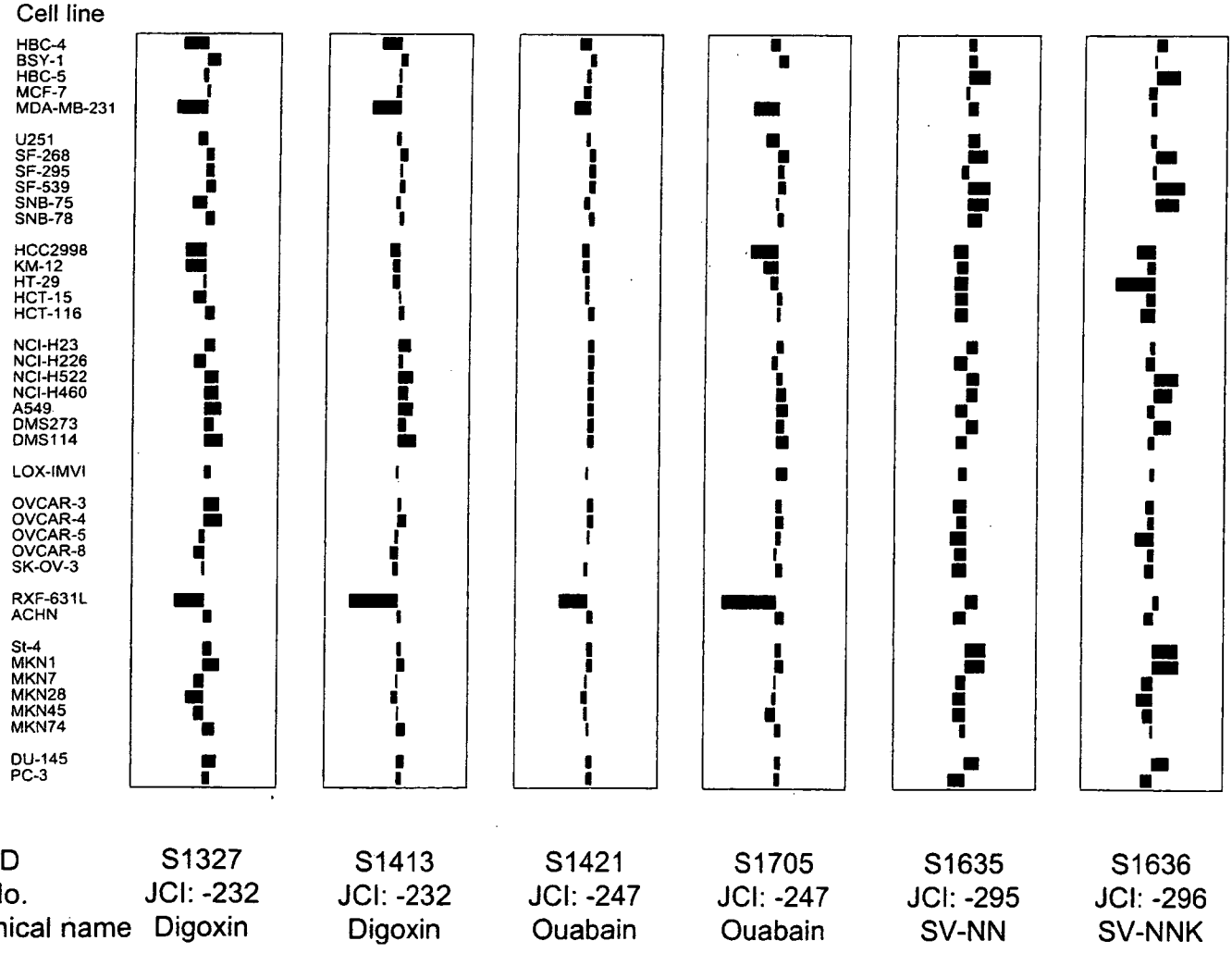

Fig. 2. Fingerprints of digoxin, ouabain, SV-NN, and SV-NNK. Fingerprint shows the differential growth inhibition pattern of the cells in the JFCR-39 panel against the test chemical. The *X*-axis represents relative value of GI50; $(-1) \times$ (log GI50 − MG-MID); MG-MID is the mean value of the log GI50. Zero means the mean GI50 and one means the GI50 value is 10-fold more sensitive than the mean GI50. Exp-ID and JCI numbers are the ID for the experiment and ID for the chemical, respectively, in our database.

10^{-6}, 10^{-7}, and 10^{-8} M) and one negative control. All assays were performed in duplicate. This GI50 calculation method is well established and reliable through anticancer drug screen using NCI60 as well as JFCR39 (Paull et al., 1989; Yamori et al., 1999; Yamori, 2003). At each test concentration, the percentage growth was calculated using the following seven absorbance measurements: growth at time 0 (T0), growth of the control cells (C), and test growth in the presence of five different concentrations (T) of a drug. The percentage growth inhibition was calculated as: % growth = 100 × [(T − T0)/(C − T0)] when T ≥ T0, and % growth = 100 × [(T − T0)/T] when T < T0. The GI50 values, which represent 50% growth inhibition concentration, were calculated as 100 × [(T − T0)/(C − T0)] = 50. When the GI50 of a chemical could not be calculated, the highest used concentration was assigned as its GI50 value. Absolute values of GI50 were then log transformed for further analysis. We certified the accuracy of measured GI50 data by using reference control chemicals, such as mitomycin-C, paclitaxel, and SN-38, in every experiment and by checking the dose response curves.

Chemicals. Spironolactone, *para*-aminoazobenzene, *para*-cresidine, neostigmine bromide, *para*-dichlorobenzene, phenytoin, *ortho*-toluidine, imipramine, cobalt chloride, atrazine, propylthiouracil, (D,L)-thalidomide, carbon tetrachloride, hydroquinone, monocrotaline, vinyl chloride, tributyl-tin chloride, valproic acid, benzene, acrylamide, pentachlorophenol, aniline, 1,3-diphenylguanidine, polypropylene glycol, 10,10′-oxy-bis(phenoxyarsine), testosterone propionate, carbaryl, acephate, bisphenol A, 17-β-estradiol, diethylstilbestrol, and α-bungarotoxin were purchased from Wako (Tokyo, Japan). Snake venoms from *Agkistrodon halys blomhoffii*, *Trimeresurus flavoviridis*, *Crotalus atrox*, *Naja nigricollis*, and *Naja naja kaouthia* were purchased from Latoxan (Valence, France). 2-Aminomethylpyridine, 1*H*-1,2,4-triazole, 1*H*-1,2,3-triazole, 3,4,4′-trichlorocarbanilide, edifenphos, dichlorvos, *O*-ethyl *O*-4-nitrophenyl phenylphosphonothioate, 2,4-dinitrophenol, *N*-methylaniline, 1,2-dichloro-3-nitrobenzene, 4-ethylnitrobenzene, 2-vinylpyridine, 3-amino-1*H*-1,2,4-triazole, *N*-ethyl-*N*-nitrosourea, 5-aza-2′- deoxycytidine, ethynyl estradiol, 3-methylcholanthrene, phenobarbital, acetaminophen, isoniazid, capsaicin, *N*-deacetyl-*N*-methylcolchicine (Colcemid), 2.4-dinitrochlorobenzene, and dexamethasone were from Sigma Chemicals (St. Louis, MO). Methoprene acid, methoprene, all-*trans* retinoic acid, and 9-cis retinoic acid were from BIOMOL International L.P. (Plymouth Meeting, PA). Levothyroxine was from MP Biomedicals (Irvine, CA). 3-Iodo-2-propynyl butylcarbamate was from Olin Japan Inc. (Tokyo, Japan), *p*-chlorophenyl-3-iodopropargylformal was from Nagase ChemteX (Osaka, Japan), and 2,3,3,3–2′,3′,3′,3′-octachlorodipropylether was from Sankyo Chemical Industries, Ltd. (Tokyo, Japan). 1,2-Benzisothiazolin-3-one was from Riverson (Osaka, Japan), zinc butylxanthate was from Ouchishinko Chemical Industrial Co., Ltd. (Tokyo, Japan), and 4-amino-2,6-dichlorophenol was from Tokyo Kasei Kogyo Co. Ltd. (Tokyo, Japan).

Hierarchical Clustering. Hierarchical clustering analysis was carried out using the average linkage method and the "GeneSpring" software (Silicon Genetics, Inc., Redwood, CA). Pearson correlation coefficients were used to determine the degree of similarity.

Results

Sensitivity of JFCR39 to Chemicals. Sensitivity of the JFCR39 panel of cells to 130 chemicals was determined as described under *Materials and Methods*. Table 1 summarizes

TABLE 2

Log_{10} GI50 values of chemicals for each cell line in the JFCR-39 panel

Hi-conc means the highest concentration of the test chemical used. When the growth inhibition was over 50% at the Hi-Conc, GI_{50} was assigned the Hi-Conc value.

Exp-ID	S3416	S3415	S3413	S3245	S3117	S3414	S3118	S3246	S3125	S3124	S3123	S1636	S1635	S1634	S1718
JCI No	−687	−686	−559	−559	−559	−560	−560	−560	−567	−566	−565	−296	−295	−294	−294
Name or Abbr.	TTNPB	13-*cis*	9-*cis*			ATRA			SV-TF	SV-CA	SV-AHB	SV-NNK	SV-NN	DTBHQ	
Hi-Conc.	−4	−4	−4	−4	−4	−4	−4	−4	−4	−4	−4	−4	−4	−4	−4
HBC-4	−4.76	−4.00	−4.53	−4.40	−4.43	−4.42	−4.41	−4.41	−5.87	−5.80	−5.66	−7.25	−7.31	−4.72	−4.80
BSY-1	−4.78	−4.16	−4.60	−4.73	−4.73	−4.69	−4.70	−4.81	−6.31	−6.06	−5.76	−6.93	−7.34	−5.07	−4.93
HBC-5	−4.80	−4.41	−4.56	−4.57	−4.61	−4.61	−4.47	−4.51	−6.98	−6.45	−5.73	−7.64	−7.72	−4.89	−4.78
MCF-7	−4.73	−4.35	−4.40	−4.39	−4.48	−4.48	−4.54	−4.66	−5.87	−5.78	−5.68	−6.77	−7.08	−5.29	−5.25
MDA-MB-231	−4.75	−4.21	−4.70	−4.55	−4.69	−4.63	−4.53	−4.65	−5.90	−5.86	−5.84	−6.84	−7.39	−5.52	−5.30
U251	−4.77	−4.14	−4.61	−4.51	−4.61	−4.57	−4.45	−4.63	−6.45	−5.76	−5.70	−6.85	−7.44	−4.96	−5.11
SF-268	−4.75	−4.00	−4.24	−4.55	−4.40	−4.47	−4.48	−4.76	−5.90	−5.79	−5.70	−7.53	−7.67	−4.77	−4.81
SF-295	−4.80	−4.29	−4.54	−4.66	−4.60	−4.59	−4.48	−4.57	−6.19	−5.80	−5.74	−6.89	−6.97	−4.87	−4.97
SF-539	−4.95	−4.35	−4.75	−4.80	−4.79	−4.80	−4.71	−4.76	−6.39	−5.96	−5.81	−7.79	−7.75	−4.79	−4.86
SNB-75	−5.31	−5.28	−5.13	−5.19		−4.71	−4.69	−4.87	−6.41	−6.33	−5.93	−7.60	−7.70	−4.67	−4.80
SNB-78	−4.77	−4.25	−4.69	−4.78	−4.86	−4.49	−4.70	−4.68	−6.19	−6.00	−5.95	−6.97	−7.53	−4.75	−4.75
HCC2998	−4.68	−4.00	−4.48	−4.61	−4.62	−4.55	−4.62	−4.76	−5.91	−5.75	−5.67	−6.47	−6.77	−4.82	−4.75
KM-12	−4.70	−4.00	−4.46	−4.51	−4.48	−4.51	−4.47	−4.58	−5.93	−5.80	−5.65	−6.77	−6.87	−4.74	−4.77
HT-29	−4.73	−4.00	−4.47	−4.53	−4.50	−4.60	−4.52	−4.56	−5.90	−5.80	−5.56	−5.89	−6.78	−4.80	−4.89
HCT-15	−4.72	−4.25	−4.45	−4.49	−4.48	−4.52	−4.57	−4.53	−5.88	−5.76	−5.57	−6.73	−6.82	−4.72	−4.77
HCT-116	−4.77	−4.07	−4.67	−4.59	−4.67	−4.71	−4.61	−4.64	−6.46	−6.10	−5.77	−6.58	−6.82	−4.98	−5.13
NCI-H23	−4.74	−4.00	−4.47	−4.60	−4.59	−4.61	−4.55	−4.63	−6.11	−5.75	−5.72	−6.86	−7.42	−4.76	−4.90
NCI-H226	−4.72	−4.00	−4.61	−4.68	−4.78	−4.80	−4.54	−5.48	−5.95	−5.81	−5.76	−6.73	−6.78	−4.89	−4.91
NCI-H522	−4.72	−4.45	−4.68	−4.82	−4.77	−4.71	−4.71	−4.68	−6.45	−5.99	−5.78	−7.62	−7.46	−5.37	−5.37
NCI-H460	−4.70	−4.00	−4.55	−4.63	−4.58	−4.68	−4.55	−4.49	−5.96	−5.82	−5.72	−7.44	−7.42	−4.84	−4.84
A549	−4.79	−4.00	−4.72	−4.77	−4.78	−4.70	−4.62	−4.53	−5.91	−5.79	−5.71	−6.80	−6.83	−4.83	−4.87
DMS273	−4.57	−4.21	−4.50	−4.62	−4.55	−4.57	−4.51	−4.49	−6.20	−5.81	−5.72	−7.43	−7.44	−4.91	−4.98
DMS114	−4.77	−4.16	−4.33	−4.62	−4.49	−4.51	−4.53	−4.61	−6.66	−6.33	−5.77	−6.83	−6.88	−5.12	−5.21
LOX-IMVI	−4.77	−4.69	−4.68	−4.66	−4.70	−4.77	−4.74	−4.74	−6.75	−6.59	−5.76	−6.86	−6.94	−5.05	−5.15
OVCAR-3	−4.77	−4.38	−4.56	−4.67	−4.72	−4.64	−4.62	−4.71	−6.61	−6.13	−5.89	−6.77	−6.79	−4.89	−4.86
OVCAR-4	−4.72	−4.05	−4.63	−4.64	−4.64	−4.58	−4.39	−4.54	−6.73	−6.23	−5.80	−6.82	−6.90	−5.13	−4.90
OVCAR-5	−4.75	−4.00	−4.33	−4.39	−4.42	−4.44	−4.34	−4.44	−5.92	−5.74	−5.67	−6.46	−6.71	−5.22	−5.26
OVCAR-8	−4.75	−4.23	−4.50	−4.53	−4.59	−4.66	−4.67	−4.70	−5.95	−5.77	−5.69	−6.82	−6.84	−4.64	−4.70
SK-OV-3	−4.79	−4.00	−4.49	−4.51	−4.81	−4.52	−4.54	−4.50	−5.76	−5.64	−4.91	−6.75	−6.76	−4.64	−4.74
RXF-631L	−4.77	−4.00	−4.54	−4.58	−4.60	−4.72	−4.63	−4.61	−5.91	−5.80	−5.59	−7.13	−7.46	−4.81	−4.84
ACHN	−4.73	−4.00	−4.56	−4.66	−4.56	−4.50	−4.40	−4.76	−5.90	−5.79	−5.73	−6.74	−6.80	−4.71	−4.83
St-4	−4.74	−4.00	−4.42	−4.54	−4.65	−4.53	−4.49	−4.57	−5.91	−5.81	−5.76	−7.65	−7.70	−4.68	−4.75
MKN1	−4.75	−4.33	−4.56	−4.63	−4.62	−4.56	−4.45	−4.48	−6.15	−5.81	−5.78	−7.67	−7.68	−4.59	−4.81
MKN7	−4.78	−4.40	−4.68	−4.59	−4.70	−4.73	−4.56	−4.65	−6.29	−5.85	−5.76	−6.70	−6.90	−4.79	−4.84
MKN28	−4.71	−4.28	−4.56	−4.59	−4.59	−4.65	−4.56	−4.60	−6.10	−5.93	−5.68	−6.51	−6.81	−4.72	−4.89
MKN45	−4.72	−4.00	−4.51	−4.41	−4.46	−4.73	−4.41	−4.43	−6.06	−5.90	−5.69	−6.71	−6.82	−4.71	−4.87
MKN74	−4.74	−4.40	−4.61	−4.63	−4.61	−4.73	−4.68	−4.67	−5.97	−5.92	−5.61	−6.92	−7.00	−5.10	−5.42
DU-145	−4.68	−4.00	−4.25	−4.78	−4.41	−4.42	−4.44	−4.54	−6.08	−5.82	−5.75	−7.43	−7.55	−4.59	−5.02
PC-3	−4.74	−4.00	−4.58	−4.65	−4.48	−4.74	−4.39	−4.51	−5.83	−5.77	−5.61	−6.67	−6.69	−4.89	−4.74

abbreviations, applications, targets, and known mechanisms of 130 chemicals and 21 anticancer drugs. Approximately 15% of the chemicals were assessed twice or more. Approximately 40% of the chemicals tested had little effect on the growth of cells in the JFCR39 panel. However, the rest of the chemicals significantly inhibited the cell growth across the JFCR39 panel. For example, Fig. 1 shows the dose response curves of the cells in the JFCR39 panel against digoxin. The concentration at which the cell growth is inhibited by 50% represents GI50. Figure 2 shows the fingerprints of four chemicals [digoxin, ouabain, snake venom from *N. nigricollis* (SV-NN), and snake venom from *N. naja kaouthia* (SV-NNK)], which differentially inhibited the growth of cells in the JFCR39 panel; these fingerprints were drawn based on a calculation using a set of GI50s and clearly represented the GI50 pattern. These results were highly reproducible in that the Pearson correlation coefficient of the duplicate experiments for digoxin was 0.839 ($p < 0.001$) and that for ouabain was 0.864 ($p < 0.001$). It is noteworthy that, digoxin and ouabain, both of which are cardiac glycosides and inhibit Na-K ATPase, showed similar fingerprints. The fingerprints of SV-NNK and SV-NN, which belong to the elapidae, known as cobras, were also similar, but were different from the fingerprints of digoxin and ouabain. Table 2 summarizes only a portion of the GI50 values from 160 experiments involving 130 chemicals and 42 experiments involving 21 anticancer drugs. GI50 values from all experiments are described in the Supplemental Data (Table S1). All these data were stored in a chemosensitivity database and used for further analysis.

Classification of the Chemicals by Hierarchical Clustering. Sixty-nine chemicals were selected for further analysis based on the following criteria: 1) GI50 values for the test chemical can be determined for at least 10 cell lines in the JFCR39 panel, and 2) the range of log GI50 for the test chemical is more than 0.6, suggesting differential growth inhibition. We analyzed the GI50 values of these 69 chemicals and 20 anticancer drugs by hierarchical clustering analysis (Fig. 3). We found approximately 12 clusters (threshold: $r = 0$, Fig. 3, clusters A–L), which were further divided into 49 subclusters (threshold: $r = 0.408$, Fig. 3, clusters A1–L6).

Analysis of Clusters. Most anticancer drugs we have tested belonged either to cluster A or cluster H, depending on their modes of action (Dan et al., 2002). The targets of the anticancer drugs belonging to the cluster A were related to DNA (Topo I, antimetabolite of pyridine, DNA alkylator) and the target of the anticancer drugs belonging to the cluster H was tubulin. We presently found that cisplatin exceptionally belonged to cluster F2, not cluster A, although it is known to cross-link DNA strands (Jamieson and Lippard, 1999; Wong and Giandomenico, 1999). We were also able to precisely group the clusters into several subclusters having similar characteristics. For example, the cardiac glycosides digoxin and ouabain were grouped in one cluster (cluster F3). SV-

S3243	S3244	S1534	S3237	S3238	S1525	S3236	S1928	S1421	S1705	S1327	S1413	S1413	S3408	S3409	S2421
−599	−599	−270	−270	−270	−261	−261	−261	−247	−247	−232	−232	−232	−421	−421	−421
Thiram		Ziram			Paraquat			Ouabain		Digoxin			TBT		
−4	−4	−4	−4	−4	−4	−3	−4	−4	−6	−4	−4	−4	−4	−4	−4
−4.71	−4.79	−5.80	−5.73	−5.70	−4.00	−3.61	−4.00	−7.54	−7.28	−6.57	−6.96	−6.96	−6.79	−6.77	−6.72
−6.97	−7.12	−6.85	−6.76	−6.60	−4.00	−4.45	−4.51	−8.00	−7.76	−7.58	−7.68	−7.68	−7.03	−7.01	−6.83
−7.41	−7.66	−7.18	−7.47	−7.47	−4.68	−4.70		−7.76	−7.51	−7.15	−7.44	−7.44	−6.76	−6.88	−6.83
−4.77	−4.80	−6.00	−5.84	−5.83	−4.06	−3.72	−4.00	−7.64	−7.51	−7.29	−7.39	−7.39	−6.86	−6.84	−6.79
−4.66	−4.68	−5.64	−5.75	−5.63	−4.00	−3.57	−4.00	−7.40	−6.81	−6.41	−6.72	−6.72	−6.83	−6.81	−6.70
−4.75	−4.78	−5.71	−5.79	−5.82	−4.00	−3.69	−4.00	−7.75	−7.16	−7.01	−7.40	−7.40	−6.79	−6.77	−6.72
−4.86	−4.96	−5.74	−5.83	−7.01	−4.00	−4.08	−4.00	−8.00	−7.77	−7.42	−7.70	−7.70	−6.84	−6.85	−6.71
−4.77	−4.89	−5.71	−5.70	−5.79	−4.47	−4.37	−4.20	−8.00	−7.64	−7.42	−7.55	−7.55	−6.75	−6.73	−6.76
−4.75	−4.88	−5.73	−5.75	−5.77	−4.00	−4.03	−4.00	−8.00	−7.70	−7.46	−7.63	−7.63	−6.77	−6.72	−6.67
−4.71	−4.96	−5.79	−5.92	−5.80	−4.00	−3.94	−4.00	−7.70	−7.45	−6.86	−7.40	−7.40	−6.99	−6.95	−7.05
−4.70	−4.78	−5.69	−5.64	−5.69	−4.00	−3.78	−4.00	−7.98	−7.64	−7.45	−7.60	−7.60	−6.72	−6.79	−6.70
−4.82	−4.69	−5.76	−5.79	−5.81	−4.00	−3.70	−4.00	−7.64	−6.77	−6.68	−7.25	−7.25	−6.77	−6.79	−6.72
−4.80	−4.80	−5.43	−5.74	−5.73	−4.00	−3.58	−4.00	−7.67	−7.12	−6.69	−7.34	−7.34	−7.00	−6.98	−6.74
−4.68	−4.85	−5.75	−5.77	−5.76	−4.10	−4.03	−4.07	−7.75	−7.31	−7.20	−7.34	−7.34	−6.89	−6.84	−6.66
−4.68	−4.75	−5.70	−5.72	−5.83	−4.00	−3.64	−4.00	−7.74	−7.63	−6.92	−7.54	−7.54	−6.88	−6.84	−6.70
−4.72	−4.72	−5.74	−5.68	−5.77	−4.00	−3.60	−4.00	−8.00	−7.57	−7.47	−7.62	−7.62	−6.90	−6.85	−6.74
−4.69	−4.78	−5.96	−5.85	−5.84	−4.19	−4.18	−4.00	−8.00	−7.67	−7.50	−7.84	−7.84	−6.90	−6.85	−6.76
−6.33	−6.74	−5.63	−5.96	−6.12	−4.41	−4.41	−4.00	−8.00	−7.37	−6.93	−7.61	−7.61	−6.99	−6.91	−6.74
−7.49	−7.50	−7.44	−7.66	−8.00	−4.49	−4.71	−4.59	−8.00	−7.64	−7.59	−7.91	−7.91	−6.83	−6.80	−6.25
−6.14	−6.16	−6.30	−6.10	−6.15	−4.30	−4.45	−4.37	−8.00	−7.74	−7.60	−7.77	−7.77	−6.98	−6.98	−6.56
−4.84	−4.82	−5.97	−5.91	−5.91	−4.49	−4.49	−4.41	−8.00	−7.80	−7.66	−7.91	−7.91	−6.82	−6.87	−6.73
−6.64	−6.58	−6.43	−6.84	−6.82	−4.25	−4.43	−4.30	−8.00	−7.71	−7.48	−7.72	−7.72	−6.74	−6.75	−6.70
−7.18	−7.39	−7.37	−7.38	−7.43	−4.50	−4.63	−4.27	−8.00	−7.84	−7.73	−8.00	−8.00	−7.11	−7.12	−7.02
−4.68	−4.71	−5.66	−5.71	−5.70	−4.00	−3.51	−4.00	−7.80	−7.80	−7.39	−7.46	−7.46	−6.93	−6.94	−6.76
−4.86	−6.25	−6.07	−6.35	−6.32	−4.00	−4.46	−4.28	−8.00	−7.66	−7.64	−7.59	−7.59	−6.80	−6.82	−6.74
−4.77	−6.67	−5.90	−5.91	−5.87	−4.00	−4.21	−4.48	−8.00	−7.71	−7.71	−7.72	−7.72	−6.91	−7.20	−6.80
−4.90	−6.00	−6.11	−6.91	−6.74	−4.00	−3.98	−4.00	−7.89	−7.62	−7.12	−7.42	−7.42	−6.90	−6.93	−6.75
−4.62	−4.74	−5.59	−5.68	−5.67	−4.00	−3.84	−4.00	−7.85	−7.44	−6.97	−7.29	−7.29	−6.73	−6.67	−6.57
−4.39	−4.38	−4.92	−5.49	−5.53	−4.00	−3.39	−4.00	−7.74	−7.67	−7.18	−7.38	−7.38	−6.80	−6.77	−6.68
−4.75	−4.65	−5.57	−5.63	−5.60	−4.00	−3.60	−4.00	−7.10	−6.00	−6.42	−6.20	−6.20	−6.78	−6.76	−6.68
−4.52	−4.60	−5.64	−5.68	−5.69	−4.00	−3.51	−4.00	−8.00	−7.72	−7.44	−7.59	−7.59	−6.78	−6.77	−6.76
−4.59	−4.72	−5.99	−5.73	−5.81	−4.00	−3.58	−4.00	−8.00	−7.65	−7.45	−7.60	−7.60	−6.80	−6.80	−6.72
−4.80	−4.85	−6.82	−5.84	−5.92	−4.41	−4.61	−4.48	−8.00	−7.72	−7.68	−7.72	−7.72	−7.25	−7.15	−6.87
−4.79	−4.82	−6.56	−5.84	−5.82	−4.08	−4.29	−4.32	−7.80	−7.48	−6.98	−7.47	−7.47	−7.34	−7.07	−6.86
−7.18	−7.21	−5.82	−7.09	−7.13	−4.00	−4.40	−4.18	−7.70	−7.42	−6.77	−7.37	−7.37	−6.84	−6.82	−6.87
−6.65	−6.71	−6.05	−7.18	−6.86	−4.00	−4.29	−4.35	−7.77	−7.25	−6.99	−7.52	−7.52	−6.96	−6.97	−6.87
−7.05	−7.08	−6.35	−5.86	−7.05	−4.00	−4.47	−4.06	−7.91	−7.65	−7.55	−7.74	−7.74	−6.97	−7.37	−7.05
−4.47	−4.70	−5.68	−5.68	−5.65	−4.00	−3.57	−4.00	−8.00	−7.64	−7.59	−7.71	−7.71	−6.90	−6.89	−6.70
−4.42	−4.77	−5.61	−5.53	−5.56	−4.00	−3.64	−4.37	−8.00	−7.62	−7.41	−7.62	−7.62	−6.77	−6.78	−6.73

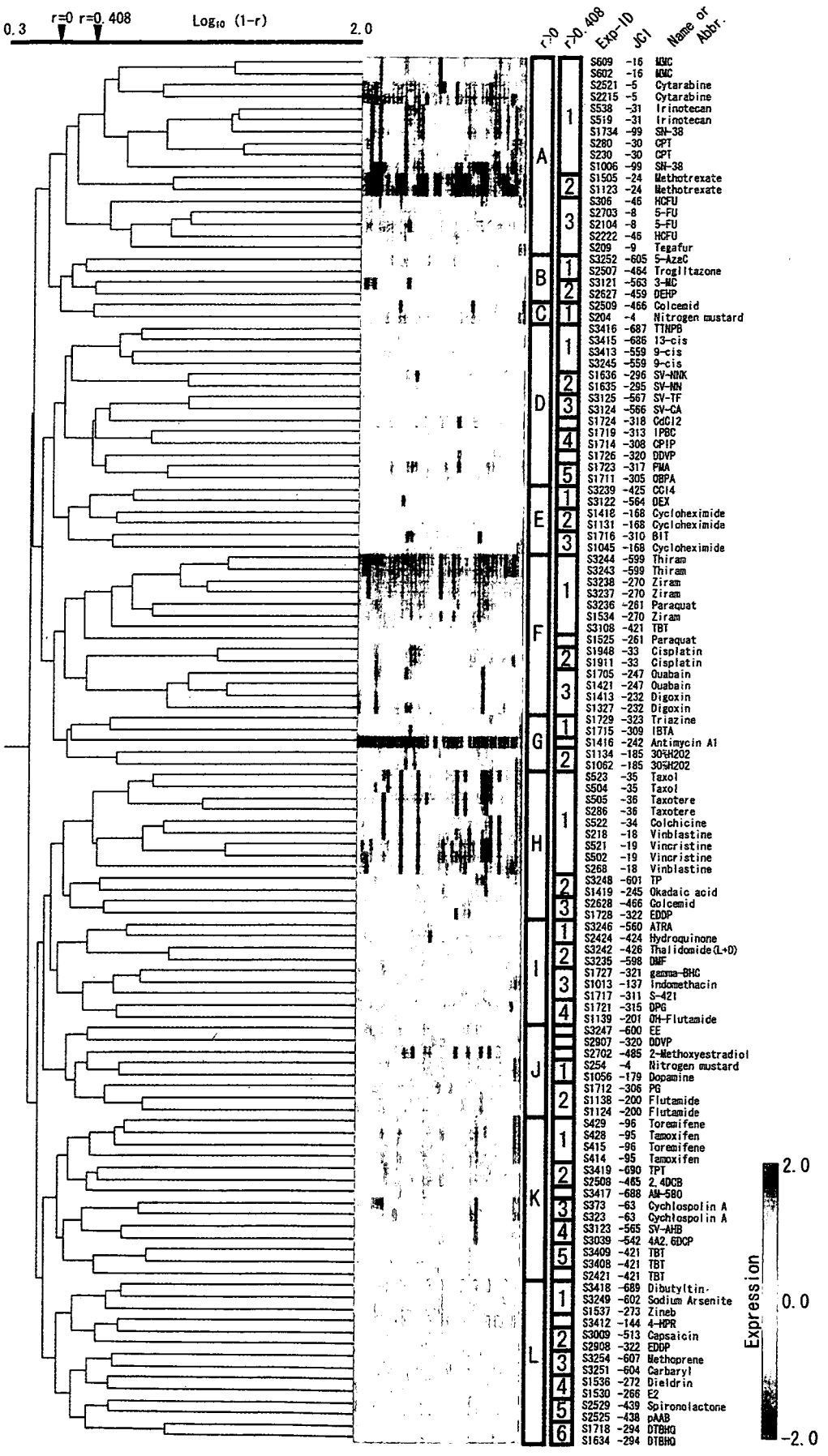

Fig. 3. Hierarchical clustering of 69 test chemicals and 20 anticancer drugs based on their GI50 values. Hierarchical clustering method was an "average linkage method" using the Pearson correlation as distance. We classified the chemicals into two kinds of clusters; their threshold values were $r = 0$ and $r = 0.408$ ($p < 0.01$), respectively. Gradient color indicates relative level (log transformed) of GI50. Red, more sensitive than the mean GI50 (2.0); yellow, mean GI50 (0.0); and green, less sensitive than the mean GI50 (−2.0). On the color scale, red represents the GI50 value that is 100-fold higher than the mean GI50.

NNK and SV-NN, on the other hand, belonged to the cluster D2. These results are in accordance with the similar fingerprints shown in Fig. 2. It is noteworthy that the snake venoms from the *C. atrox* and *T. flavoviridis*, species belonging to the viperidae family of snakes, formed another cluster (cluster D3), which was different from that of the elapidae family of snakes, *N. naja kaouthia* and *N. nigricollis*. 9-*cis* Retinoic acid, 13-*cis* retinoic acid, and 4-[*E*-2-(5,6,7,8-tetrahydro-5,5,8,8-tetra-methyl-2-naphthalenyl)-1-propenyl]benzoic acid, which are RAR agonists (Aström et al., 1990), also formed a separate cluster (cluster D1). Likewise, agricultural chemicals paraquat, ziram, and thiram formed a single cluster (cluster F1).

Discussion

The JFCR39 system coupled to a drug activity database is a good model for investigating the diversity of chemosensitivity in cancer cells. We have previously established panels of human cancer cell lines [JFCR39 (Yamori, 2003) and JFCR45 (Nakatsu et al., 2005)]. We used these panels of cells to demonstrate that they provide powerful means to predict the action mechanisms of drugs, and also used them to identify new target compounds. In this manuscript, we used the JFCR39 system to evaluate various chemicals (such as toxic chemicals, agricultural chemicals, and synthetic intermediates), which are not anticancer drugs, and classified them according to their molecular target or action mechanism. As a result, these chemicals were classified into a number of clusters. Our results also suggested that each cluster consisted of chemicals sharing a common action mechanism.

We determined the growth inhibition of cells in the JFCR39 panel by 130 chemicals and calculated their GI50 values. Some of the chemicals were assessed twice or more to confirm the reproducibility of the assay. We had to exclude 61 chemicals from further analysis because they did not inhibit the cells in the JFCR39 panel significantly. The rest of the chemicals (69 of 130, ~60%) met our selection criteria and were evaluated by cluster analysis.

First, we found that the chemicals tested in duplicate formed tight clusters, showing high reproducibility. Next, we investigated the difference between these 69 test chemicals and the anticancer drugs. Sixty-nine chemicals, which are not anticancer drugs, formed several clusters, which were different from the anticancer drug clusters. These results suggest that the action mechanisms of these chemicals are different from the action mechanisms of the anticancer drugs. However, we found that cisplatin did not belong to the cluster A, which consisted of DNA-targeting anticancer drugs. We do not understand the reason at present. However, there is a possibility that cisplatin has other action mechanisms, which may have made the fingerprint of cisplatin different from those of other DNA-targeting drugs. Indeed, cisplatin is known to form DNA-protein cross-links (Zwelling et al., 1979; Chválová et al., 2007).

Our analysis also identified several interesting clusters. For example, the cluster F3 consisted of cardiac glycosides digoxin and ouabain, both of which inhibit Na-K ATPase (Reuter et al., 2002). The cluster D1 consisted of 9-*cis* retinoic acid, 13-*cis* retinoic acid, and 4-[*E*-2-(5,6,7,8-tetrahydro-5,5,8,8-tetra-methyl-2-naphthalenyl)-1-propenyl]benzoic acid, which are RAR agonists. These results suggest that chemicals other than the anticancer drugs also form clusters when they share the same action mechanisms. It is noteworthy that SV-NNK and SV-NN, from snakes that belonged to the elapidae family, formed one cluster (cluster D2). In contrast, the snake venoms from the *C. atrox* and *T. flavoviridis*, which belonged to the viperidae family, formed a cluster (cluster D3) different from the elapidae cluster. These results are reasonable because snake venoms from different snake families are known to differ not only in composition but also in levels of toxicity and mechanisms of action.

The agricultural chemicals paraquat, ziram, and thiram were also classified into a single cluster (cluster F1). Among these agricultural chemicals, the action mechanism of ziram is not known. However, both paraquat and thiram are known to induce oxidative stress (Cereser et al., 2001; Suntres, 2002). Therefore, based on our observations, we could suggest that ziram also acted by inducing oxidative stress. The agricultural chemicals methoprene (insect growth regulator) and carbaryl (chorine esterase inhibitor) formed cluster L3, although their common mechanism is unknown. Cluster D4 and D5 consist of the antibacterial agents or fungicides. 3-Iodo-2-propynyl-butylcarbamate and *p*-chlorophenyl-3′-iodopropargylformal, belonging to cluster D4, are the iodo-type antibacterial agents.

Thus, cluster analysis of GI50 values of various chemicals, determined using the JFCR39 cell panel, suggests that the JFCR39 system could, at least in part, allow classification of chemical compounds on the basis of their action mechanisms. Our analysis also suggests that the chemicals belonging the same cluster share a common action mechanism. We are going to develop a larger library of reference chemicals with known action mechanisms (i.e., various inhibitors of biological pathways), and expand our database by integrating their GI50 measurements, which will make the cluster analysis as well as the COMPARE analysis more informative for predicting the mechanism of test chemicals.

In conclusion, to evaluate the potential of the JFCR39 system in predicting the action mechanisms of toxic chemicals, we investigated the fingerprints of 130 different types of chemical compounds including toxic chemicals, pesticides, drugs, and synthetic intermediates. Using the hierarchical clustering analysis, we classified 69 chemicals, at least in part, based on their action mechanisms. Thus, this approach using the JFCR39 cell panel is useful not only in predicting the action mechanisms of toxic chemicals but also in evaluating their toxicity.

Acknowledgments

We thank Yumiko Mukai, Yumiko Nishimura, and Mariko Seki for determination of chemosensitivity and Satoshi Kitajima for help with chemical information.

References

Akashi T, Nishimura Y, Wakatabe R, Shiwa M, and Yamori T (2007) Proteomics-based identification of biomarkers for predicting sensitivity to a PI3-kinase inhibitor in cancer. *Biochem Biophys Res Commun* **352**:514–521.

Akashi T and Yamori T (2007) A novel method for analyzing phosphoproteins using SELDI-TOF MS in combination with a series of recombinant proteins. *Proteomics* **7**:2350–2354.

Aström A, Pettersson U, Krust A, Chambon P, and Voorhees JJ (1990) Retinoic acid and synthetic analogs differentially activate retinoic acid receptor dependent transcription. *Biochem Biophys Res Commun* **173**:339–345.

Cereser C, Boget S, Parvaz P, and Revol A (2001) An evaluation of thiram toxicity on cultured human skin fibroblasts. *Toxicology* **162**:89–101.

Chválová K, Brabec V, and Kasparkova J (2007) Mechanism of the formation of DNA-protein cross-links by antitumor cisplatin. *Nucleic Acids Res* **35**:1812–1821.

Dan S, Shirakawa M, Mukai Y, Yoshida Y, Yamazaki K, Kawaguchi T, Matsuura M, Nakamura Y, and Yamori T (2003) Identification of candidate predictive markers of anticancer drug sensitivity using a panel of human cancer cell lines. *Cancer Sci* **94**:1074–1082.

Dan S, Tsunoda T, Kitahara O, Yanagawa R, Zembutsu H, Katagiri T, Yamazaki K, Nakamura Y, and Yamori T (2002) An integrated database of chemosensitivity to 55 anticancer drugs and gene expression profiles of 39 human cancer cell lines. *Cancer Res* **62**:1139–1147.

Hershberger LG, Shipley EG, and Meyer RK (1953) Myotrophic activity of 19-nortestosterone and other steroids determined by modified levator ani muscle method. *Proc Soc Exp Biol Med* **83**:175–180.

Jamieson ER and Lippard SJ (1999) Structure, Recognition, and Processing of Cisplatin-DNA Adducts. *Chem Rev* **99**:2467–2498.

Kanno J, Kato H, Iwata T, and Inoue T (2002) Phytoestrogen-low diet for endocrine disruptor studies. *J Agric Food Chem* **50**:3883–3885.

Naasani I, Seimiya H, Yamori T, and Tsuruo T (1999) FJ5002: a potent telomerase inhibitor identified by exploiting the disease-oriented screening program with COMPARE analysis. *Cancer Res* **59**:4004–4011.

Nakamura H, Dan S, Akashi T, Unno M, and Yamori T (2007) Absolute quantification of four isoforms of the class I phosphoinositide-3-kinase catalytic subunit by real-time RT-PCR. *Biol Pharm Bull* **30**:1181–1184.

Nakatsu N, Yoshida Y, Yamazaki K, Nakamura T, Dan S, Fukui Y, and Yamori T (2005) Chemosensitivity profile of cancer cell lines and identification of genes determining chemosensitivity by an integrated bioinformatical approach using cDNA arrays. *Mol Cancer Ther* **4**:399–412.

Okutsu J, Tsunoda T, Kaneta Y, Katagiri T, Kitahara O, Zembutsu H, Yanagawa R, Miyawaki S, Kuriyama K, Kubota N, et al. (2002) Prediction of chemosensitivity for patients with acute myeloid leukemia, according to expression levels of 28 genes selected by genome-wide complementary DNA microarray analysis. *Mol Cancer Ther* **1**:1035–1042.

Paull KD, Shoemaker RH, Hodes L, Monks A, Scudiero DA, Rubinstein L, Plowman J, and Boyd MR (1989) Display and analysis of patterns of differential activity of drugs against human tumor cell lines: development of mean graph and COMPARE algorithm. *J Natl Cancer Inst* **81**:1088–1092.

Reuter H, Henderson SA, Han T, Ross RS, Goldhaber JI, and Philipson KD (2002) The Na^+-Ca^{2+} exchanger is essential for the action of cardiac glycosides. *Circ Res* **90**:305–308.

Scherf U, Ross DT, Waltham M, Smith LH, Lee JK, Tanabe L, Kohn KW, Reinhold WC, Myers TG, Andrews DT, et al. (2000) A gene expression database for the molecular pharmacology of cancer. *Nat Genet* **24**:236–244.

Suntres ZE (2002) Role of antioxidants in paraquat toxicity. *Toxicology* **180**:65–77.

Weinstein JN, Kohn KW, Grever MR, Viswanadhan VN, Rubinstein LV, Monks AP, Scudiero DA, Welch L, Koutsoukos AD, and Chiausa AJ (1992) Neural computing in cancer drug development: predicting mechanism of action. *Science* **258**:447–451.

Weinstein JN, Myers TG, O'Connor PM, Friend SH, Fornace AJ Jr, Kohn KW, Fojo T, Bates SE, Rubinstein LV, Anderson NL, et al. (1997) An information-intensive approach to the molecular pharmacology of cancer. *Science* **275**:343–349.

Wong E and Giandomenico CM (1999) Current status of platinum-based antitumor drugs. *Chem Rev* **99**:2451–2466.

Yaguchi S, Fukui Y, Koshimizu I, Matsuno T, Gouda H, Hirono S, Yamazaki K, and Yamori T (2006) Antitumor activity of ZSTK474, a new phosphatidyl inositol 3-kinase inhibitor. *J Natl Cancer Inst* **98**:545–556.

Yamori T (2003) Panel of human cancer cell lines provides valuable database for drug discovery and bioinformatics. *Cancer Chemother Pharmacol* **52 (Suppl 1)**: S74–S79

Yamori T, Matsunaga A, Sato S, Yamazaki K, Komi A, Ishizu K, Mita I, Edatsugi H, Matsuba Y, Takezawa K, et al. (1999) Potent antitumor activity of MS-247, a novel DNA minor groove binder, evaluated by an in vitro and in vivo human cancer cell line panel. *Cancer Res* **59**:4042–4049,.

Zembutsu H, Ohnishi Y, Tsunoda T, Furukawa Y, Katagiri T, Ueyama Y, Tamaoki N, Nomura T, Kitahara O, Yanagawa R, et al. (2002) Genome-wide cDNA microarray screening to correlate gene expression profiles with sensitivity of 85 human cancer xenografts to anticancer drugs. *Cancer Res* **62**:518–527.

Zwelling LA, Anderson T, and Kohn KW (1979) DNA-protein and DNA interstrand cross-linking by cis- and trans-platinum(II) diamminedichloride in L1210 mouse leukemia cells and relation to cytotoxicity. *Cancer Res* **39**:365–369.

Address correspondence to: Takao Yamori, Division of Molecular Pharmacology, Cancer Chemotherapy Center, Japanese Foundation for Cancer Research, 3-10-6, Ariake, Koto-ku, Tokyo 135-8550, Japan. E-mail: yamori@jfcr.or.jp, 07a$sl

0888-8809/06/$15.00/0
Printed in U.S.A.

Molecular Endocrinology 20(9):2141–2155

doi: 10.1210/me.2005-0367

Endocrine-Disrupting Organotin Compounds Are Potent Inducers of Adipogenesis in Vertebrates

Felix Grün, Hajime Watanabe, Zamaneh Zamanian, Lauren Maeda, Kayo Arima, Ryan Cubacha, David M. Gardiner, Jun Kanno, Taisen Iguchi, and Bruce Blumberg

Department of Developmental and Cell Biology (F.G., Z.Z., L.M., K.A., R.C., D.M.G., B.B.), University of California Irvine, Irvine California 92697-2300; National Institutes of Natural Sciences (H.W., T.I.), National Institute for Basic Biology, Okazaki Institute for Integrative Bioscience, Okazaki 444-8787, Japan; and Division of Cellular & Molecular Toxicology (J.K.), Biological Safety Research Center, National Institute of Health Sciences, Setagaya-ku, Tokyo 158-8501, Japan

Dietary and xenobiotic compounds can disrupt endocrine signaling, particularly of steroid receptors and sexual differentiation. Evidence is also mounting that implicates environmental agents in the growing epidemic of obesity. Despite a long-standing interest in such compounds, their identity has remained elusive. Here we show that the persistent and ubiquitous environmental contaminant, tributyltin chloride (TBT), induces the differentiation of adipocytes *in vitro* and increases adipose mass *in vivo*. TBT is a dual, nanomolar affinity ligand for both the retinoid X receptor (RXR) and the peroxisome proliferator-activated receptor γ (PPARγ). TBT promotes adipogenesis in the murine 3T3-L1 cell model and perturbs key regulators of adipogenesis and lipogenic pathways *in vivo*. Moreover, *in utero* exposure to TBT leads to strikingly elevated lipid accumulation in adipose depots, liver, and testis of neonate mice and results in increased epididymal adipose mass in adults. In the amphibian *Xenopus laevis*, ectopic adipocytes form in and around gonadal tissues after organotin, RXR, or PPARγ ligand exposure. TBT represents, to our knowledge, the first example of an environmental endocrine disrupter that promotes adipogenesis through RXR and PPARγ activation. Developmental or chronic lifetime exposure to organotins may therefore act as a chemical stressor for obesity and related disorders. (*Molecular Endocrinology* 20: 2141–2155, 2006)

ORGANOTINS ARE A diverse group of widely distributed environmental pollutants. Tributyltin chloride (TBT) and bis(triphenyltin) oxide (TPTO), have pleiotropic adverse effects on both invertebrate and vertebrate endocrine systems. Organotins were first used in the 1960s as antifouling agents in marine shipping paints, although such use has been restricted in recent years. Organotins persist as prevalent contaminants in dietary sources, such as fish and shellfish, and through pesticide use on high-value food crops (1, 2). Additional human exposure to organotins may occur through their use as antifungal agents in wood treatments, industrial water systems, and textiles. Mono- and diorganotins are prevalently used as stabilizers in the manufacture of polyolefin plastics (polyvinyl chloride), which introduces the potential for transfer by contact with drinking water and foods.

Exposure to organotins such as TBT and TPTO results in imposex, the abnormal induction of male sex characteristics in female gastropod mollusks (3, 4). Bioaccumulation of organotins decreases aromatase activity leading to a rise in testosterone levels that promotes development of male characteristics (5). Imposex results in impaired reproductive fitness or sterility in the affected animals and is one of the clearest examples of environmental endocrine disruption. TBT exposure also leads to masculinization of at least two fish species (6, 7), but TBT is only reported to have modest adverse effects on mammalian male and female reproductive tracts and does not alter sex ratios (8, 9). Instead, hepatic-, neuro-, and immunotoxicity appear to be the predominant effects of organotin exposure (10). Hence, the current mechanistic understanding of the endocrine-disrupting potential of organotins is based on their direct actions on the levels or activity of key steroid-regulatory enzymes such as aromatase and more general toxicity mediated via damage to mitochondrial functions and subsequent cellular stress responses (11–15).

However, it remains an open question whether *in vivo* organotins act primarily as protein and enzyme

First Published Online April 13, 2006

Abbreviations: Acac, Acetyl-coenzyme A carboxylase; b.w., body weight; C/EBP, CCAAT/enhancer binding protein; 9-*cis* RA, 9-cis retinoic acid; DMSO, dimethylsulfoxide; F, forward; Fatp, fatty acid transport protein; LBD, ligand-binding domain; LXR, liver X receptor; MDIT, 3-isobutyl-1-methylxanthine, dexamethasone, insulin and T_3 adipocyte differentiation mix; PPAR, peroxisome proliferator-activated receptor; R, reverse; RAR, retinoic acid receptor; RXR, retinoid X receptor; Srebf1, sterol-regulatory element binding factor 1; TBT, tributyltin chloride; TPTO, triphenyltin oxide; TTNPB, (E)-4-[2-(5,6,7,8-tetrahydro-5,5,8,8-tetramethyl-2-naphthylenyl)-1-propenyl] benzoic acid; VDR, vitamin D receptor.

***Molecular Endocrinology* is published monthly by The Endocrine Society (http://www.endo-society.org), the foremost professional society serving the endocrine community.**

inhibitors, or rather mediate their endocrine-disrupting effects at the transcriptional level. Recent work has shown that aromatase mRNA levels can be down-regulated in human ovarian granulosa cells by treatment with organotins or ligands for the nuclear hormone receptors, retinoid X receptor (RXRs) or peroxisome proliferator-activated receptor γ (PPARγ) (16–18). Furthermore, Nishikawa *et al.* (19) have demonstrated that the gastropod *Thais clavigara* RXR homolog is responsive to 9-cis-retinoic acid (9-*cis*-RA) and TBT, and 9-*cis* RA can also induce imposex, suggesting a conserved transcriptional mechanism for TBT action across phyla. These ligand-dependent transcription factors belong to the nuclear hormone receptor superfamily—a group of approximately 150 members (48 human genes) that includes the estrogen receptor, androgen receptor, glucocorticoid receptor, thyroid hormone receptor, vitamin D receptor (VDR), retinoic acid receptors (RARs and RXRs), PPARs, and numerous orphan receptors. We were therefore intrigued by the similar effects of TBT and RXR/PPARγ ligands on mammalian aromatase mRNA expression and hypothesized that TBT might be exerting some of its biological effects via transcriptional regulation of gene expression through activation of one or more nuclear hormone receptors.

Our results show that organotins such as TBT are indeed potent and efficacious agonistic ligands of the vertebrate nuclear receptors, retinoid X receptors (RXRs) and PPARγ. The physiological consequences of receptor activation predict that permissive RXR heterodimer target genes and downstream signaling cascades are sensitive to organotin misregulation. Consistent with this prediction we observe that organotins phenocopy the effects of RXR and PPARγ ligands using *in vitro* and *in vivo* models of adipogenesis. Therefore, TBT and related organotin compounds are the first of a potentially new class of environmental endocrine disrupters that targets adipogenesis by modulating the activity of key regulatory transcription factors in the adipogenic pathway, RXRα and PPARγ. The existence of such xenobiotic compounds was previously hypothesized (20, 21). Our results suggest that developmental exposure to TBT and its congeners that activate RXR/PPARγ might be expected to increase the incidence of obesity in exposed individuals and that chronic lifetime exposure could act as a potential chemical stressor for obesity and obesity-related disorders.

RESULTS

Organotins Are Agonists of Vertebrate RXR and RXR-Permissive Heterodimers

Many known or suspected environmental endocrine-disrupting chemicals mimic natural lipophilic hormones that act through members of the superfamily of nuclear receptor transcription factors (22, 23). In a screen of high-priority endocrine-disrupting chemicals against a bank of vertebrate nuclear receptor ligand-binding domains (LBDs), we observed that organotins, specifically tributyltin chloride (TBT) and bis(triphenyltin) oxide (TPTO), could fully activate an RXRα LBD construct (GAL4-RXRα) in transient transfection assays. Both TBT and TPTO were as potent (EC_{50} ~3–10 nM) as 9-*cis* retinoic acid, an endogenous RXR ligand and approximately 2- to 5-fold less potent than the synthetic RXR-specific ligands LG100268 (EC_{50} ~ 2 nM) or AGN195203 (EC_{50} ~ 0.5 nM) (Fig. 1A and see Table 2). Maximal activation for TBT reached the same levels as LG100268 or AGN195203.

We next tested whether activation by TBT was unique to RXRα only, restricted to RXR heterodimer complexes, or a general nuclear receptor transcriptional response (Fig. 1, B–D, and Table 1). TBT activated RXRα and RXRγ from the amphibian *Xenopus laevis* in addition to human RXRs (Table 1). Our results are consistent with recent findings by Nishikawa *et al.* (19, 24) that organotins promote activation of all three human RXR subtypes in a yeast two-hybrid screen. We also observed significant activation of receptors typically considered to be permissive heterodimeric partners of RXR including human PPARγ (Fig. 1B, ~30% maximal activation of 10 μM troglitazone, but note that activation is compromised by cellular toxicity above 100 nM), PPARδ, liver X receptor (LXR), and the orphan receptor NURR1. In contrast, typical nonpermissive partners such as RARs, thyroid hormone receptor, and VDR failed to show activation by organotins (Fig. 1C and Table 1). Murine PPARα was also not activated by TBT although it was fully activated by its specific synthetic agonist WY-14643 (Fig. 1D). The steroid and xenobiotic receptor was likewise unresponsive. The orphan receptor NURR1, which has no discernable ligand pocket and is believed to be ligand independent (25), was nevertheless activated 7- to 10-fold at 100 nM TBT. Similarly, other RXR-specific ligands, *e.g.* LG100268, activated NURR1 to the same degree, suggesting that this response occurred through NURR1's heterodimeric partner RXR as has been previously described (25, 26). Like other RXR-specific ligands, tributyltin was also able to promote the ligand-dependent recruitment of nuclear receptor cofactors such as receptor-associated coactivator 3 (ACTR), steroid receptor coactivator-1, and PPAR-binding protein in mammalian two-hybrid interaction assays (data not shown). We infer from these results that nuclear receptor activation by TBT activation is specific to a small subset of receptors and not a consequence of a general effect on the cellular transcriptional machinery.

We next investigated the relationship between the structure of the tin compounds and RXR activation by testing the response of GAL4-RXRα to mono-, di-, tri-, and tetra-substituted butyltin, branched side chains, variations in the alkyl chain length, and changes in the halide component (Fig. 1A and Table 2). Overall, trialkyltin compounds were the most effective with nano-

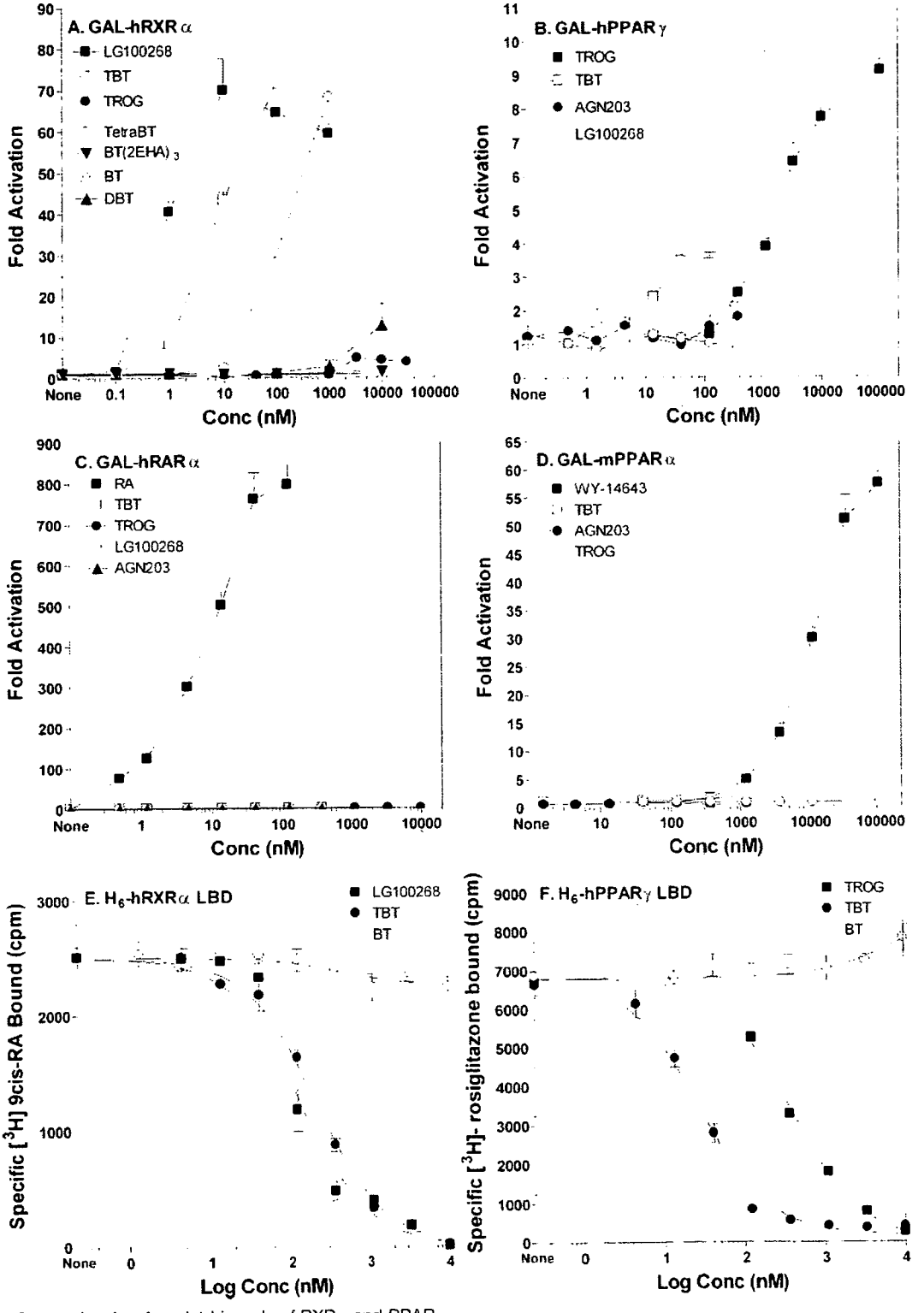

Fig. 1. Organotins Are Agonist Ligands of RXRα and PPARγ

Organotins are high-affinity ligand agonists of RXRα and PPARγ. A–D, Activation of GAL4-hRXRα, -hPPARγ, -hRARα, or -hPPARα in transiently transfected Cos7 cells by organotins and receptor-specific ligands. Data represent reporter luciferase activity normalized to β-galactosidase and plotted as the average fold activation ± SEM (n = 3) relative to solvent-only controls from representative experiments. E and F, Competition binding curves of histidine-tagged RXRα or PPARγ LBDs with TBT. Data shown are from a representative experiment analyzed in GraphPad Prism 4.0 and K_i values deduced (Table 3). Conc, Concentration; DBT, dibutyltin chloride; TROG, troglitazone.

Table 1. TBT Activates RXRs and RXR-Permissive Heterodimers

GAL4-NR LBD	Fold Activation at 60 nM TBT	Permissive RXR Heterodimer
RXRα (*Homo sapiens*)	60	Yes
RXRα (*X. laevis*)	25	Yes
RXRγ (*X. laevis*)	7.0	Yes
NURR1 (*H. sapiens*)	7.0	Yes
LXR (*H. sapiens*)	2.1	Yes
PPARα (*Mus musculus*)	0.7	Yes
PPARγ (*H. sapiens*)	5.3	Yes
PPARδ (*H. sapiens*)	1.7	Yes
RARα (*H. sapiens*)	0.7	No
TR&β (*H. sapiens*)	0.4	No
VDR (*H. sapiens*)	0.5	No
SXR (*H. sapiens*)	1.0	No

Data are fold activation at 60 nM TBT relative to solvent-only controls of transiently transfected Cos7 cells after 24 h ligand treatment. SXR, Steroid and xenobiotic receptor; TR, thyroid hormone receptor.

molar EC_{50} values. Monobutyltin gave no significant activation whereas dibutyltin was moderately active in the micromolar range (Fig. 1A and Table 2). Tetrabutyltin was 20-fold less potent than TBT, whereas the branched side-chain butyltin tris(2-ethylhexanoate) [BT(2-EHA)$_3$] was inactive (Table 2). Although activation by dialkyltins is weaker than that of TBT, it is potentially significant due to their widespread use in the manufacture of polyvinyl chloride plastics and greater solubility than TBT.

The effect of the hydrocarbon chain length was very pronounced, suggesting an important structure-activity relationship. A reduction in hydrophobicity from butyl to ethyl side chains raised the EC_{50} value by almost 1000-fold into the micromolar range. Trimethyltin was weakly active only above 100 μM (Table 2). Substitution of the halide component had no significant effect on the EC_{50} values for TBT, probably due to the lability of the halide atom through exchange in aqueous tissue culture media where chloride ions are prevalent.

Table 2. Organotin EC_{50} Values for Nuclear Receptor LBDs

Ligand	GAL4-NR LBD Transactivation (EC_{50} Values, nM)		
	hRXRα	hRARα	hPPARγ
LGD268	2–5	na	na
AGN195203	0.5–2	na	na
9-*cis* RA	15	na	na
all-*trans* RA	na	8	na
Butyltin chloride	na	na	na
Dibutyltin chloride	3000	na	na
TBT	3–8	na	20
Tetrabutyltin	150	ND	ND
Di(triphenyltin)oxide	2–10	na	20
Butyltin tris(2-ethylhexanoate)	na	ND	ND
Troglitazone	na	na	1000
Tributyltin fluoride	3	ND	ND
Tributyltin bromide	4	ND	ND
Tributyltin iodide	4	ND	ND
Triethyltin bromide	2800	ND	ND
Trimethyltin chloride	>10000	ND	ND

na, Not active; ND, not determined. EC_{50} values were determined from dose-response curves of GAL4-NR LBD construct activation in transiently transfected Cos7 cells after 24-h ligand exposure.

TBT Is a Potent Ligand of Both RXRα and PPARγ

Many, if not most, natural and synthetic nuclear receptor agonists act as ligands that specifically interact with their cognate receptor LBDs. We therefore performed equilibrium competition binding experiments with purified histidine-tagged human RXRα (H_6-RXRα) and PPARγ (H_6-PPARγ) LBDs to determine whether the potent and specific activation of these receptors by TBT was due to direct ligand-receptor interaction (Fig. 1, E and F).

The equilibrium binding curves indicate that TBT is a high-affinity, competitive ligand for 9-*cis* RA-bound RXRα. The inhibition equilibrium dissociation constant was calculated by the Chang-Prusoff method [inhibition constant (K_i) = dissociation constant (K_d)] as 12.5 nM (10–15 nM; 95% confidence interval) (Table 3). By comparison, the value obtained for the synthetic RXR agonist LG100268 was 7.5 nM, which compared favorably with its published value of approximately 3 ± 1 nM (27). Therefore, the identification of TBT as an RXR ligand expands the molecular definition of known rexinoids (agonists able to activate RXR) to include this structurally unique class of organotin compounds.

Somewhat surprisingly, we also observed potent specific competitive binding by TBT for rosiglitazone bound to human PPARγ LBD (Fig. 2B). The deduced K_i of 20 nM (17–40 nM; 95% confidence interval) was slightly higher than for RXRα but significantly better than the K_i for the PPARγ agonist troglitazone, which

Table 3. TBT Binding Constants (K_d) for hRXRα and hPPARγ LBDs

Ligand	Receptor Competitive Inhibition Binding Constants K_i (nM ± 95% CI)		
	H_6-RXRα	H_6-PPARγ	Published
TBT	12.5 (10–15)	20 (17–40)	
LG100268	7.5 (6–10)	ND	3 ± 1[a]
Troglitazone	ND	300 (270–335)	300 ± 30[b]

Competition binding curves were determined at constant ^{3}H-specific ligand concentrations [20 nM 9-*cis*-RA, K_d = 1.4 nM (87) or rosiglitazone, K_d = 41 nM (88)] with increasing cold competitor ligands over the range indicated in Fig. 1, E and F. Data were analyzed in GraphPad Prism by nonlinear regression of a competitive one-site binding equation (Chang-Prusoff method) to determine K_i values ± 95% confidence intervals (n = 3). CI, Confidence interval; ND, not determined.
[a] RXRα:LG100268 K_d = 3 ± 1 nM (27).
[b] PPARγ:troglitazone K_d = 300 ± 30 nM (28).

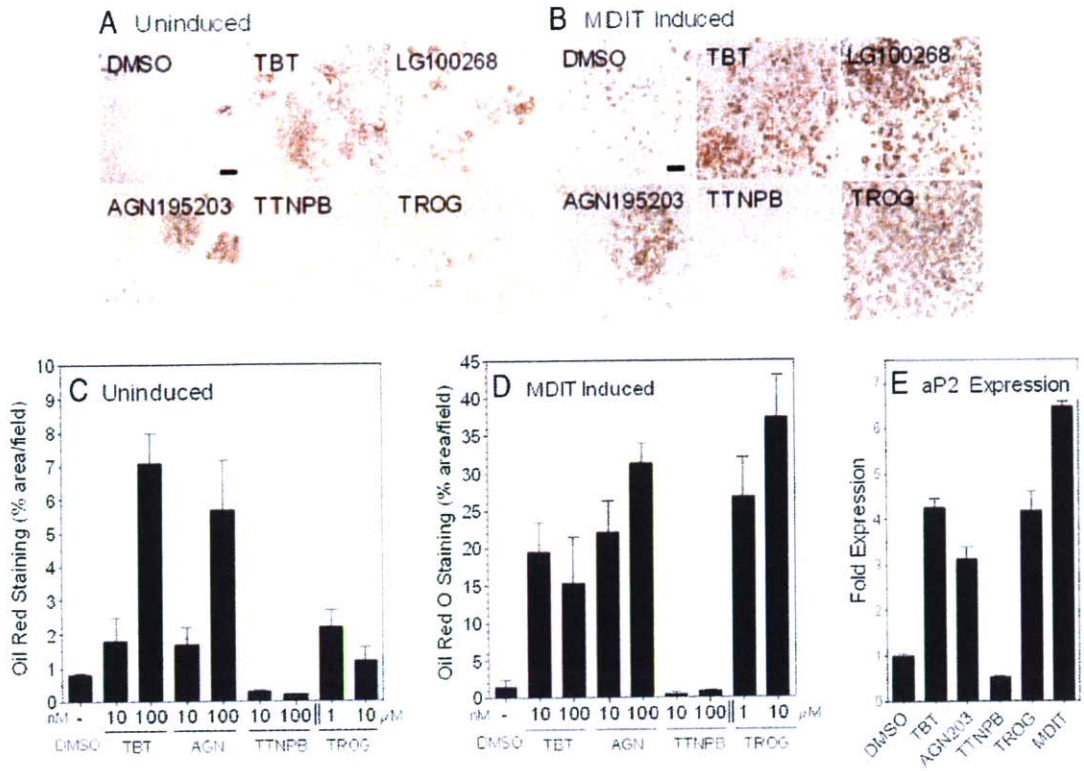

Fig. 2. Tributyltin Induces Adipogenesis in 3T3-L1 Cells

Uninduced (A) and MDIT-induced (B) 3T3-L1 cultures grown for 1 wk in the presence of vehicle (DMSO), or ligands were analyzed for mature adipocyte differentiation by Oil Red O staining. *Scale bar* represents 100 μm. C and D, The percentage area stained was determined by automated analysis of random fields (n = 9) from high-contrast dissecting scope photographs of monolayers analyzed in ImageJ; 1–100 nM of TBT, AGN195203, and TTNPB or 1–10 μM troglitazone. E, Quantitative real-time PCR (QRT-PCR) of adipocyte-specific fatty acid binding protein aP2 (aP2/Fabp4) expression levels in postconfluent 3T3-L1 cells treated with the indicated ligands for 24 h. Data were normalized to glyceraldehyde-3-phosphate dehydrogenase controls and plotted as average fold induction ± SEM (n = 3).TROG, Troglitazone.

yielded a K_i of 300 nM, consistent with its published K_d (28). The K_d values for TBT binding to RXRα (12.5 nM) and PPARγ (20 nM) are also in close agreement with EC_{50} values obtained from transient transfection assays using GAL4-RXRα and GAL4-PPARγ constructs (Table 2).

Taken together, these data show that organotins such as TBT, although structurally distinct from previously described natural or synthetic ligands, can interact with RXRα and PPARγ, via direct ligand binding to induce productive receptor-coactivator interactions and promote transcription in a concentration-dependent manner. Organotins are therefore potent nanomolar receptor activators on par with synthetic RXR and PPARγ ligands such as LG100268, AGN195203, and thiazolidinediones.

TBT Promotes Adipogenesis in the Murine 3T3-L1 Cell (Embryonic Murine Preadipocyte Fibroblast Cell Line) Model

Numerous studies have demonstrated the critical role played by RXRα:PPARγ signaling in regulation of mammalian adipogenesis (29–31). In the murine 3T3-L1 preadipocyte cell model, adipogenic signals induce early key transcriptional regulators such as CCAAT/enhancer binding proteins (C/EBPs) β and δ that lead to mitotic clonal expansion of growth-arrested preadipocytes and induction of the late differentiation factors C/EBPα and PPARγ (32–34). The combination of C/EBPα expression together with PPARγ signaling efficiently drives terminal adipocyte differentiation and lipid accumulation. We therefore tested whether TBT signaling through RXR:PPARγ could promote adipogenesis in the murine 3T3-L1 differentiation assay and compared its effect to other RXR-specific or PPARγ ligands (Fig. 2). Undifferentiated 3T3-L1 cells were cultured for 1 wk in the presence of ligands either with or without a prior 2-d treatment with MDIT (an adipogenic-sensitizing cocktail of 3-isobutyl-1-methylxanthine, dexamethasone, insulin, and T_3) (35). Cells were then scored for lipid accumulation using Oil Red O staining to determine the degree of terminal adipocyte differentiation. TBT was as effective as LG100268 or AGN195203 in promoting dif-

ferentiation in the absence of MDIT treatment, increasing the number of differentiated adipocytes about 7-fold over solvent-only controls (Fig. 2, A and C). The PPARγ agonist troglitazone was a weak inducer in the absence of MDIT. Prior treatment with MDIT increased the response to TBT, LG100268, and AGN195203 a further 3- to 5-fold (Fig. 2, B and D). MDIT treatment also boosted the response to troglitazone to equivalent levels as expected from published studies showing that combination treatment with PPARγ ligands promotes efficient adipocyte differentiation (36–38). In contrast, the RAR agonist TTNPB inhibited the differentiation of 3T3-L1 cells, consistent with previously published data that showed RAR signaling blocks adipogenesis during the early stages of differentiation *in vitro* and can modulate adiposity and whole body weight *in vivo* (39–41). The differential response of 3T3-L1 cells to receptor-selective retinoids indicates that TBT favors RXR homodimer or permissive RXR-heterodimer rather than RXR:RAR signaling in this cell model.

Adipocyte differentiation by TBT was accompanied by direct transcriptional effects on RXR:PPARγ targets such as adipocyte-specific fatty acid-binding protein (aP2) mRNA. The aP2 promoter contains response elements sensitive to C/EBP factors and RXRα:PPARγ signaling (42). Quantitative real-time PCR analysis showed aP2 levels were elevated by TBT treatment approximately 5-fold at 24 h (Fig. 2E) and 45-fold at 72 h (data not shown). LG100268, troglitazone, and MDIT treatment also increased aP2 expression at these time points whereas the RAR agonist TTNPB was inhibitory, consistent with the observed cellular responses.

TBT Induces Adipogenic Regulators and Markers of RXRα:PPARγ Signaling *in Vivo*

The ability of organotins to regulate RXRα:PPARγ target genes and key modulators of adipogenesis and lipid homeostasis *in vivo* has not been previously examined. Therefore, we next asked whether TBT could perturb expression of critical transcriptional mediators of adipogenesis such as RXRα, PPARγ, C/EBPα/β/δ, and sterol regulatory element binding factor 1 (Srebf1) as well as known target genes of RXRα:PPARγ signaling from liver, epididymal adipose tissue, and testis of 6-wk-old male mice dosed for 24 h with TBT [0.3 mg/kg body weight (b.w.)], AGN195203 (0.3 mg/kg b.w.), troglitazone (3 mg/kg b.w), or vehicle (corn oil) administered by ip injection. TBT either had no effect or weakly repressed RXRα and PPARγ transcription in liver (Fig. 3, A and B). A more pronounced decrease was observed for RXRα, PPARγ, C/EBPα, and C/EBPδ in adipose tissue and testis (Fig. 3, B and C). In contrast, TBT, AGN195203, and troglitazone significantly induced expression of the early adipogenic transcription factor C/EBPβ in liver and testis, whereas it was more weakly induced in adipose tissue. Induction was strongest in testis where TBT and troglitazone increased expression greater than 10-fold and AGN195203 increased expression 60-fold compared with vehicle controls (Fig. 3C). In addition to C/EBPβ, the proadipogenic transcription factor Srebf1 was also significantly increased in adipose tissue by all three receptor ligands and weakly induced in liver.

We also observed coordinate changes in several well-characterized direct target genes of RXR:PPARγ signaling. Fatty acid transport protein (Fatp) acts as a key control point for regulation of cellular fatty acid content. The Fatp promoter contains a functional PPAR response element shown to be sensitive to RXR:PPARγ signaling in 3T3-L1 adipocytes and white fat (43–46). Fatp mRNA levels were up regulated 2- to 3-fold in liver and epididymal adipose tissue but not testis by TBT, AGN195203, and troglitazone (see Fig. 5, A and B). Similarly, the PPARγ target phosphoenolpyruvate carboxykinase 1 (PEPCK/Pck1) (47), the rate-limiting step in hepatic gluconeogenesis and adipose glyceroneogenesis, was up-regulated in liver and adipose tissues by TBT or troglitazone treatment.

Signaling through RXR:PPARγ, RXR:LXR, and ADD1/Srebf1 in hepatocytes has been shown to modulate fatty acid synthesis through transcriptional control of acetyl-coenzyme A carboxylase (Acac), the rate-limiting step in long-chain fatty acid synthesis (48, 49), as well as fatty acid synthase (Fasn) (50–53). Hepatic expression of both Acac and Fasn was unregulated between 1.5–2.5-fold by TBT, AGN195203, and troglitazone. Therefore, the coordinate increased expression of Fatp, Pck1, Acac, and Fasn in liver suggests that TBT stimulates fatty acid uptake and triglyceride synthesis. Similar changes have been reported in the induction of hepatic steatosis by overactive PPARγ signaling (49, 54).

Taken together, these data show that TBT exposure induces lipogenic RXR:PPARγ target gene expression, in adipose tissue and liver, and modulates associated early adipocyte differentiation factors such as C/EBPβ and Srebf1. We inferred from these data that organotins are potential adipogenic agents *in vivo*.

Developmental Exposure to TBT Disrupts Lipid Homeostasis and Adipogenesis in Vertebrates

Based on its molecular pharmacology, ability to induce 3T3-L1 adipocyte differentiation, and *in vivo* transcriptional responses, we reasoned that TBT would disrupt normal endocrine control over lipid homeostasis and impact adipogenesis, particularly when exposure occurred during sensitive periods of development. We therefore tested this hypothesis in two vertebrate model systems, mouse and *X. laevis*, during embryogenesis.

Pregnant C57BL/6 mice were injected daily from gestational d 12–18 with TBT (0.05 or 0.5 mg/kg body weight ip) dissolved in sesame oil or vehicle alone. Pups were then killed at birth, and histological sections were prepared from liver, testis, mammary gland, and inguinal adipose tissue. Sections were stained

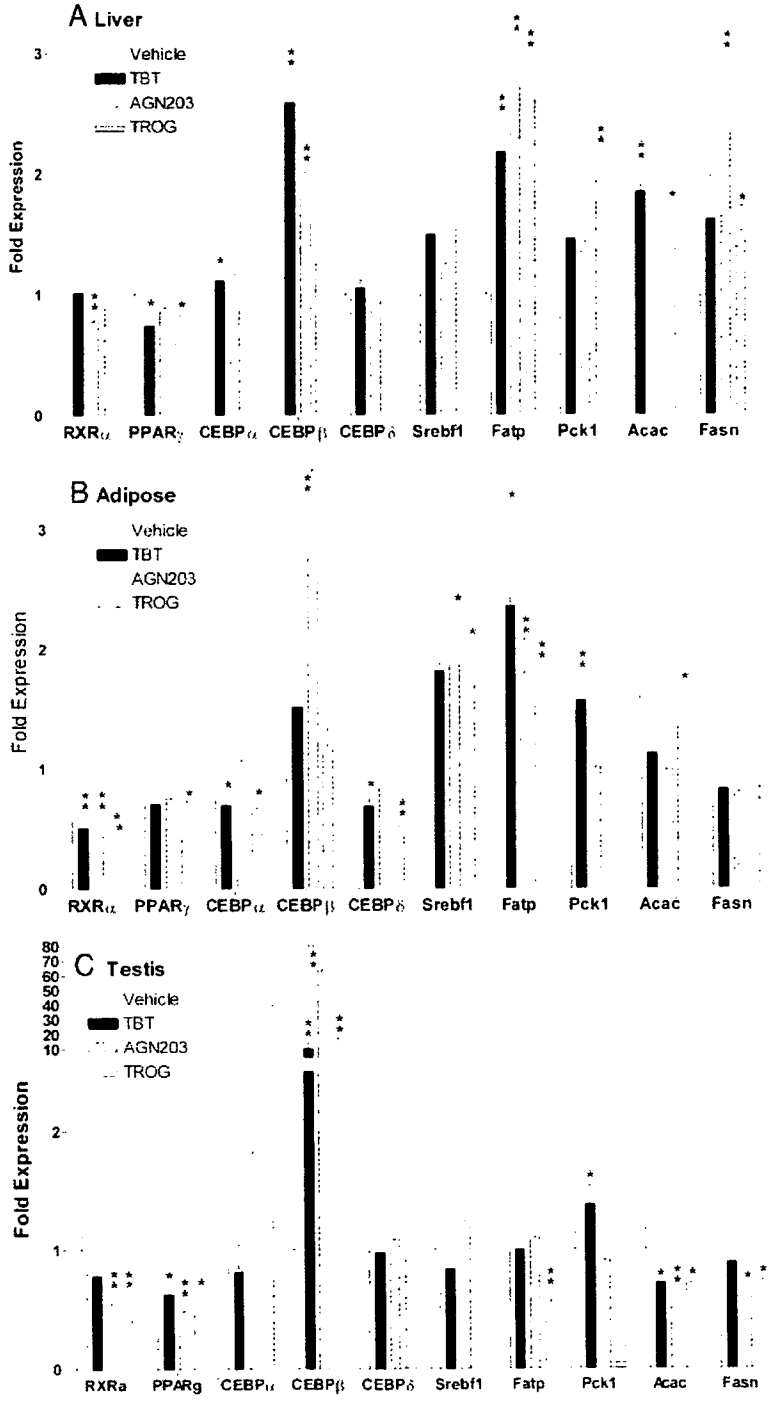

Fig. 3. *In Vivo* Induction of Adipogenic Modulators and RXR:PPARγ Target Genes

C57BL/6 male mice (three animals per treatment) were dosed with TBT (0.3 mg/kg b.w.), AGN195203 (0.3 mg/kg), troglitazone (3 mg/kg b.w.), or vehicle (corn oil) only by ip injection. Animals were killed after 24 h and dissected and cDNA was prepared from liver, epididymal fat pad, or testis for quantitative real-time PCR analysis. Expression levels were normalized to histone Hist2h4 and shown as the average fold change ± SEM (n = 3) compared with vehicle (corn oil) controls. Control *vs.* ligand treatments were analyzed by the unpaired Student's *t* test: *, $P < 0.1$; **, $P < 0.05$. TROG, Troglitazone.

with Oil Red O to assess changes in total tissue lipid accumulation. TBT exposure caused a disorganization of hepatic (Fig. 4, A and B) and gonadal (Fig. 4, C and D) architecture and significantly increased Oil Red O staining in treated animals *vs.* controls. Liver sections exhibited signs of steatosis consistent with the mis-

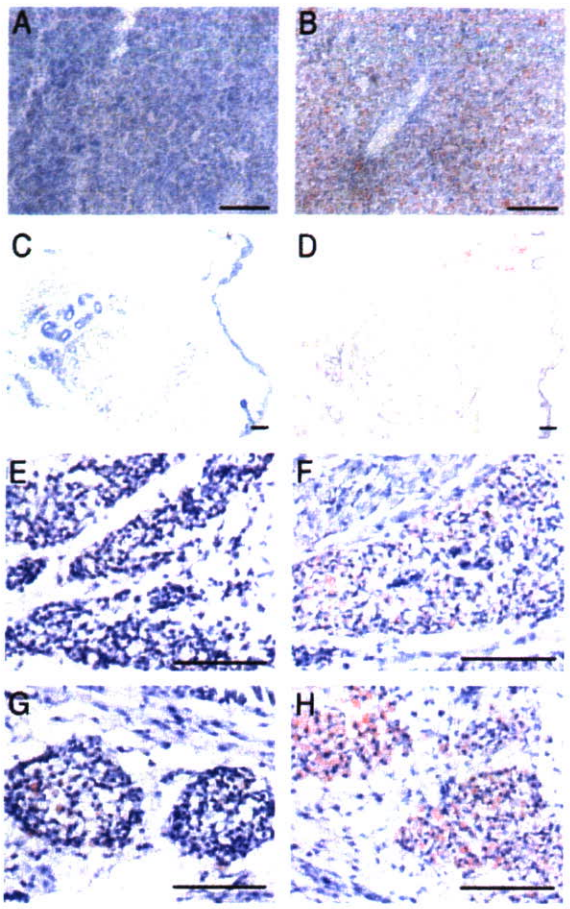

Fig. 4. *In Utero* Exposure to TBT Increases Adiposity in Mouse Liver, Testis, and Adipose Depots

Histological sections (12 μm) of newborn mouse liver (A and B), testis (C and D), inguinal adipose (E and F) and mammary adipose (G and H) stained with Oil Red O and counterstained with hematoxylin following *in utero* exposure to vehicle only (sesame oil) (A, C, E, and G) or 0.5 mg/kg b.w. TBT (B, D, F, and H) given s.c. daily from E12–18. *Scale bar*, 100 μm.

regulation of fatty acid uptake and synthesis observed using molecular markers. In addition, Oil Red O positive staining in mammary and inguinal adipose (Fig. 4, E–H) tissues was dramatically elevated, reflecting either an increase in lipid accumulation or an increase in mature adipocytes.

To determine whether exposure induced long-term changes in growth or adipose tissue, we followed mice from birth to adulthood after *in utero* exposure to TBT as indicated above. At birth, mice were cross-fostered to unexposed dams, and total body weight was recorded until 10 wk of age (Fig. 5A). Growth curves for male and female pups showed a slight trend for lower total body weight consistent with published observations (9) but were not statistically significant at 10 wk [control *vs.* TBT: male, 26.00 g ± 0.70 (n = 9) *vs.* 25.53 g ± 0.39 (n = 10), $P = 0.583$; female, 21.22 g ± 0.41 (n = 10), *vs.* 20.24 g ± 0.24 (n = 10), $P = 0.0529$]. Males were killed at 10 wk and epididymal fat pads were weighed (Fig. 5B). Adipose mass in TBT-treated males was increased significantly by 20% over controls [control *vs.* TBT: 0.30 g ± 0.020 (n = 9) *vs.* 0.36 g ± 0.018 (n = 10), $P = 0.0374$]. These data support the conclusion that TBT can increase body adiposity without overtly increasing total body weight. Similar lipid accumulation and changes in adipose tissue mass have also been observed after TZD or rexinoid treatment (55–57).

We had previously observed that TBT activated *Xenopus* RXRs (Table 1) and reasoned that the strong conservation in vertebrate nuclear receptor signaling pathways should result in consistent responses to organotin and RXR/PPARγ ligands across diverse vertebrate species. We therefore tested chronic exposure to environmentally relevant low doses of TBT (1–10 nM), the RXR-specific ligands LG100268 and AGN195203 (10–100 nM), troglitazone (0.1–1 μM), and estradiol (1–10 nM) on developing *X. laevis* tadpoles from stage 48 to metamorphs. To determine the effectiveness of these doses in *X. laevis* tadpoles, we used aromatase expression as a molecular marker because activity and expression are sensitive to endocrine disruption by organotins and RXR/PPARγ ligands in mammals (17, 18). *Xenopus* aromatase expression was similarly repressed 2- to 3-fold by 10 nM TBT, AGN195203, LG100268, or 1 μM troglitazone at stage 56 tadpoles (Fig. 6A) and at all subsequent stages. Despite significant ligand-induced aromatase down-regulation, neither sex ratios nor the time required to reach metamorphosis was altered (data not shown). *Xenopus* liver and kidney also exhibited no gross structural abnormalities at the doses given.

However, consistent with the testis and adipose results from mice presented above, we observed a dose-dependent increase in ectopic adipocyte formation posterior to the fat bodies in and around the gonads of both sexes after TBT or RXR/PPARγ ligand exposure (Fig. 6B). In contrast, estradiol-treated animals did not show increased adipocyte formation compared with controls. At 10 nM TBT, 10 nM AGN195203, or 1 μM troglitazone, ectopic adipocytes were observed in approximately 45–60% of animals. At the highest dose of TBT in males, testicular tissue was interspersed with, or replaced by, adipocytes along the anterior-posterior axis (Fig. 6, D, E, and G).

The concordant changes observed in *Xenopus* aromatase expression, gonadal adipocyte formation, and increased murine adiposity after exposure to TBT, RXR and PPARγ ligands are therefore consistent with a common mechanism of action through RXR:PPARγ activation, supporting the conclusion that endocrine disruption via nuclear receptor transcriptional regulation is a novel and key feature of organotin toxicity.

DISCUSSION

We have shown above that TBT is a potent inducer of adipogenesis, *in vitro* and *in vivo*, by acting as a novel,

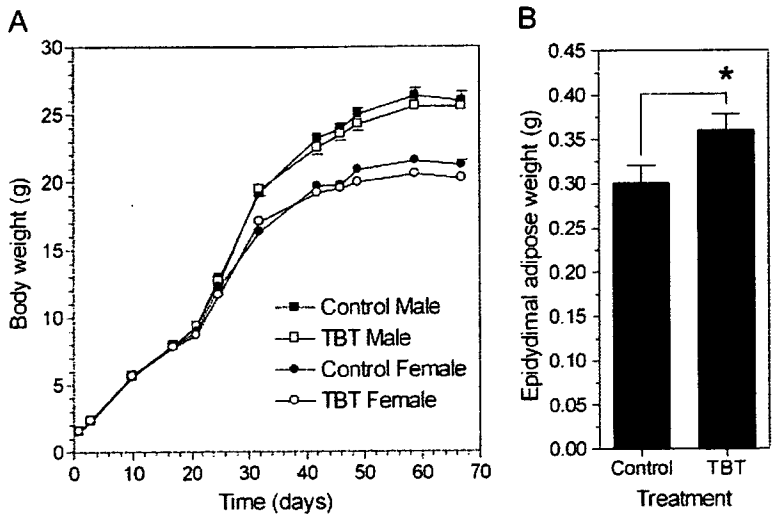

Fig. 5. *In Utero* Exposure to TBT Increases Adipose Mass But Not Body Weight in Adult Mice

A, Growth curves of C57BL/6 male and female pups exposed to control (sesame oil) or TBT *in utero* (E12–18). Data are mean ± SEM (n = 10). B, Epididymal fat pad weights from control or TBT-treated males at 10 wk. *, Epididymal adipose mass from exposed males was approximately 20% greater [control *vs.* TBT: 0.30 g ± 0.020 (n = 9) *vs.* 0.36 g ± 0.018 (n = 10); *, $P = 0.0374$). Data represent mean ± SEM (n = 9–10).

high-affinity xenobiotic ligand for RXRα and PPARγ. The ability of organotins to bind and activate these receptors, in particular the RXRs, which exhibit very restricted ligand specificity, is unexpected given the radically different chemical composition and three-dimensional molecular structure of organotins when compared with known natural and synthetic nuclear receptor ligands. Typically, RXR ligands comprise a carboxylic acid functional group and a three-dimensional molecular shape that mimics 9-*cis* RA. Structure-activity profiles indicate distinct structural preferences for organotins but also a relatively broad accommodation for agonist activity that is not easily reconciled with the classical ligand-binding model. Organotins may therefore interact somewhat differently than previously described RXR/PPARγ ligands with receptor LBDs to induce productive conformational changes required for coactivator recruitment. However, the binding data indicate that TBT is a potent and efficacious ligand for both RXRs and PPARγ that interacts, at least partially, with the same receptor-binding sites of other high-affinity ligands and promotes the necessary cofactor interactions required for agonist activation. In the study of Kanayama *et al.* (24), TBT was only effective in coactivator recruitment assays with PPARγ above 10 μM *in vitro*. However, in accord with our findings, they show that TBT activated PPARγ significantly at nanomolar concentrations in transfection assays. This may reflect a limitation of preference in the cofactor used *in vitro*. Alternatively, the lower maximal activation observed with TBT on PPARγ in cells (~30% at 100 nM TBT cf troglitazone) is consistent with one of two possibilities: either nonspecific cellular toxicity at high levels or activation as a partial agonist.

The ability of TBT to act as a dual ligand for permissive heterodimers such as RXRα:PPARγ, which can be activated by specific ligands for either receptor, also raises the possibility for additive or synergistic effects that might increase the potency of these compounds *in vivo* at low doses for this specific signaling pathway. Of note is that receptor activation is observed at nanomolar concentrations, whereas other mechanisms of toxicity and endocrine disruption, *e.g.* direct inhibition of aromatase activity, typically occur in the micromolar range. Furthermore, the activation of other permissive RXR heterodimeric partners, *e.g.* LXR and NURR1, suggests that organotins may act more widely to disrupt multiple nuclear receptor-mediated hormonal signaling pathways.

The biological consequences of organotin activation of the RXR:PPARγ signaling pathway are predictable and should follow known aspects of RXR/PPARγ biology. The RXR:PPARγ pathway plays a key role in adipocyte differentiation and energy storage, and is central to the control of whole-body metabolism (58). PPARγ activation increases the expression of genes that promote fatty acid storage and represses genes that induce lipolysis in adipocytes in white adipose tissue (59). PPARγ such as the thiazolidinediones can modulate insulin sensitivity due to these effects on the adipocyte, reversing insulin resistance in the whole body by sensitizing the muscle and liver tissue to insulin (60). However, a consequence of this increase in whole-body insulin sensitivity is that fat mass is increased through the promotion of triglyceride storage in adipocytes. Evidence is also mounting that depot-specific remodeling and adipocyte numbers increase after thiazolidinedione treatment (55–57). Therefore, PPARγ agonists comprise a class of phar-

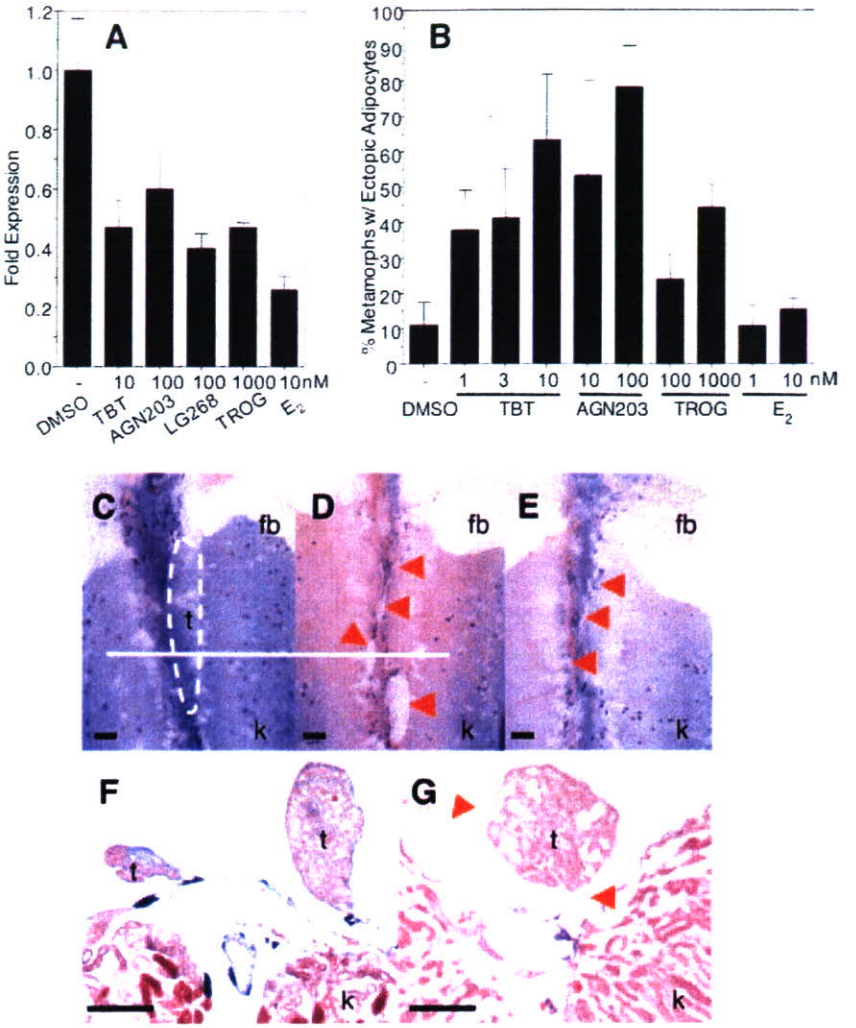

Fig. 6. Endocrine Disruption of RXR:PPARγ Signaling and Ectopic Induction of Adipocytes in *X. laevis* by TBT

A, Expression levels of *Xenopus* aromatase (XCYP19) were determined in tadpoles (stage 56) by quantitative real-time PCR after 24-h exposure to vehicle only (DMSO) or the indicated ligands. Expression was normalized to *Xenopus* EF1α and expressed as average fold change in expression ± SEM (n = 9) relative to vehicle controls. B, *X. laevis* tadpoles were dosed weekly under static renewal conditions with indicated ligands from stage 48 (before gonadogenesis) until stage 64 (metamorphic climax). Metamorphs (stage 66) were scored for ectopic adipocyte patches on gonads and urogenital ducts. Data are shown as the percentage of metamorphs exhibiting ectopic adipocyte patches posterior to the fat bodies; mean ± SD from triplicate tanks. C–E, Dissecting microscope photographs of kidneys (k), testis (t), and fat bodies (fb) from DMSO control, 10 nM TBT, and 1 μM troglitazone-treated male metamorphs. Multiple ectopic adipocyte patches (*red arrows*) are present posterior to the fat bodies along the anterior-posterior axis of gonads in TBT (D)- and troglitazone (E)-treated animals but not controls (C). Histological sections of kidneys and gonads from the same control (F) and 10 nM TBT (G)-treated males at the level indicated by the *white line* in C and D. Gonadal and connective tissue was either completely replaced by, or interspersed with, adipocytes (*red arrows*) in TBT-treated animals. Sections were developed with Mallory's trichrome stain. *Scale bars*, 100 μm.

maceutical therapies for type 2 diabetes that can also promote obesity by increasing fat storage. Likewise, RXR ligands also act as insulin-sensitizing agonists in rodents (61), underscoring the permissive nature of the PPARγ:RXR heterodimer and the potential effects on diabetes and obesity of both PPARγ and RXR agonists.

Our data are consistent with recent studies that organotins can mediate some of their endocrine disruption effects by transcriptional regulation through nuclear receptors, in particular RXR:PPARγ signaling (17–19, 24). Consequently, TBT exposure can promote adipocyte differentiation in the same manner as other RXR or PPARγ ligands *in vitro* using the standard murine 3T3-L1 cell model and *in vivo* through increased adiposity after intrauterine organotin exposure in newborn mice. It is currently unknown whether the increased adiposity *in vivo* results from an increase

in adipocyte precursor cell number, enhanced adipocyte differentiation from the same number of precursors, an increase in adipocyte size without an increase in number, or some combination of these.

The prevailing epidemiological data ascribe high-density caloric and/or fatty diets coupled with decreased physical activity as the root causes for the rise in obesity rates in the general population (62). The contribution of genetic components is less clear. Although genetic variation contributes to an individual's propensity to develop obesity, the rapid worldwide increase in obesity suggests that interaction with the modern environment exposes inherent genetic differences. The Barker hypothesis postulates that *in utero* fetal nutritional status is a potential risk factor for metabolic syndrome diseases (63–67). In this view, developmental metabolic programming of a thrifty phenotype limits the range in adaptive responses to the environment, *e.g.* diet and exercise, in later life (68). Experimental evidence from animal models lends support to this hypothesis (69). Plausible mechanisms include imprinting of obesity-sensitive hormonal pathways or changes in cell type and number, *e.g.* adipocytes, established during development.

Others, however, argue that the environment plays another role in obesity. Because the increase in obesity rates parallels the rapid growth in the use of industrial chemicals over the past 40 yr, it is plausible and provocative to associate *in utero* or chronic lifetime exposure to chemical triggers present in the modern environment with this epidemic. Hence, an "obesogen" model predicts the existence of xenobiotic chemicals that inappropriately regulate lipid metabolism and adipogenesis to promote obesity. Several recent studies serve as proof-of-principle for such a hypothesis. Environmental estrogens such as bisphenol A and nonylphenol, for instance, can promote adipocyte differentiation or proliferation in murine cell lines (70, 71). Furthermore, epidemiological studies link maternal smoking during pregnancy to an elevated risk of childhood obesity (72–76).

Seen in this context, we propose that organotins such as TBT and its congeners are chemical stressors or obesogens that activate RXR:PPARγ signaling to promote long-term changes in adipocyte number and/or lipid homeostasis after developmental or chronic lifetime exposure.

MATERIALS AND METHODS

Plasmids and Transfections

pCMX-GAL4 and pCMX-VP16 plasmid fusion constructs to nuclear receptor LBDs and coactivators [GAL4-hRARα, hRXRα, -xRXRα/γ, -hPPARγ, -mPPARα, -human steroid and xenobiotic receptor (SXR), -NURR1, -VDR, -LXR, -hACTR, -hPPAR-binding protein (PBP), -human steroid receptor coactivator-1 (SRC-1), human transcriptional intermediary factor 2 (TIF2)] have been previously described (77–82). Transfections were performed in Cos7 cells (transformed green monkey kidney fibroblast cell line) essentially as described elsewhere (83) using MH200-x4-TK-Luc as reporter and normalized to pCMX-β-galactosidase controls. Briefly, Cos7 cells were seeded at 5000 cells per well in 96-well tissue culture plates in 10% fetal bovine serum/DMEM and transfected for 8 h with 11 μg/plate of DNA/calcium phosphate precipitate mix (MH200x4-TK-Luc-CMX-β-galactosidase-nuclear receptor/coactivator effector(s) at a ratio of 5:5:1). Cells were washed free of precipitate with PBS and media were replaced with serum-free insulin, transferrin, lipid, bovine serum albumin supplemented (ITLB)/DMEM (84) plus ligands for an additional 24 h before assays for luciferase and β-galactosidase activity. All transfection data points were performed in triplicate, and all experiments were repeated at least three times.

Quantitative Real-Time PCR Analyses

Total cellular RNA from C57BL/6 mouse and *X. laevis* tissues was isolated with Trizol reagent and reversed transcribed with oligo dT and Superscript II (Invitrogen, San Diego, CA) according to the manufacturer's instructions. Triplicate cDNA samples (50 ng/reaction) were analyzed by quantitative real-time PCR on a DNA Engine Opticon thermal cycler [MJ Research (Watertown, MA)/Bio-Rad Laboratories (Hercules, CA)] using SYBR Green chemistry (PerkinElmer Life Sciences, Wellesley, MA). Fold changes in expression levels were calculated after normalization to histone Hist2h4 using the Δ-Δ cycle threshold method (85). Gene-specific primers were as follows. Hist2h4 forward (F): 5′-CCCGTGGTGTGCTGAAGGTGTT-3′; reverse (R), 5′-GAATTGAAGCGGCGGCGTCTA-3′; RXRα F: 5′-CGGCTGCTCAGGGTACTTGTGTTT-3′; R, 5′-CGGCTGCTCAGGGTACTTGTGTTT-3′; PPARγ F: 5′-TGGGTGAAACTCTGGGAGATTC-3′; R, 5′-AATTTCTTGTGAAGTGCTCATAGGC-3′; C/EBPα F: 5′-CCAAGAAGTCGGTGGACAAGA-3′; R, 5′-CGGTCATTGTCACTGGTCAACT-3′; C/EBPβ F: 5′-GCCCGCCGCCTTTAGACC-3′; R, 5′-CGCTCGTGCTCGCCAATG-3′; C/EBPδ F: 5′-AACCCGCGGCCTTCTACGAG-3′; R, 5′-ACGGCGGCCATGGAGTCAAT-3′; aP2 F: 5′-GAATTCGATGAAATCACCGCA-3′; R, 5′-CTCTTTATTGTGGTCGACTTTCCA-3′; FATP F: 5′-AGCCGCTTCTGGGATGACTGTGT-3′; R, 5′-ACCGAAGCGCTGCGTGAACTC-3′; ACS F: 5′-CCCAGCCAGTCCCCACCAG-3′; R, 5′-CACACCACTCAGGCTCACACTCGT-3′; FASN F: 5′-TCGGGTGTGGTGGGTTTGGTGAAT-3′; R, 5′-ACTTGGGGGCGTGAGATGTGTTGC-3′;ACAC F: 5′-G GATGGCAGCTCTGGAGGTGTATG-3′; R, 5′-TGTCCTTAAGCTGGCGGTGTTGTA; Pck1 F: 5′-CTGGCAGCATGGGGTGTTTGTAGG-3′; R, 5′-TGCCGAAGTTGTAGCCGAAGAAGG-3′; Srebf1 F: 5′-GCCCCTGCCCACCTCAAACCT-3′; R, 5′-ACTGGCACGGGCATCCTTCCTC-3′; *Xenopus* EF1α F: 5′-GATCCCAGGAAAGCCAATGTGC 3′; R, 5′-CCGGATCCTGCTGCCTTCTTCT-3′; *Xenopus* CYP19 (aromatase) F: 5′-GTCTGGATTAATGGCGAGGAAACA-3′; R, 5′-CTGATGAAGTATGGCCGAATGACC-3′.

Ligand Binding

Histidine-tagged RXRα LBD (H_6-RXRα LBDs) was expressed and purified from pET15b(+) vector in BL21(DE3) pLysS bacteria cultures after induction with 1 mM isopropyl-β-D-thiogalactopyranoside for 3 h at 37 C (86). Purified H_6-PPARγ was purchased from Invitrogen. Proteins were bound to 96-well Nickel Chelate Flashplates (PerkinElmer Life Sciences) at 100 μg/ml overnight at 4 C and washed five times with 200 μl/well Flashplate Assay Buffer (20 mM HEPES, pH 7.9; 100 mM KCl, 0.1% cholamidopropyldimethylammonio-2-hydroxy-1-propanesulfonate, 0.1 mM dithiothreitol). Competition assays typically used 1–5 nM [^{3}H]-9-*cis*-RA (PerkinElmer Life Sciences) or 10–50 nM [^{3}H]rosiglitazone (American Radiochemicals, Inc., St. Louis, MO) plus cold competitor ligands in Flashplate Assay Buffer at concentrations indicated in the figures. Plates were incubated at room temperature, pro-

tected from light, and read after 4 h on a Packard Topcount scintillation counter (Packard Instruments, Meriden, CT). Specific bound counts/min were determined by subtraction of counts/min from uncoated wells at each ligand concentration. Data were analyzed with GraphPad Prism 4.0 (GraphPad Software, Inc., San Diego, CA) using a one-site competition binding equation to determine K_i values for competitor ligands; K_d values of 1.4 and 41 nM for 9-*cis*-RA and rosiglitazone for their respective receptors were used in the calculations (87, 88).

3T3-L1 Cell Assays

3T3-L1 (American Type Culture Collection, Manassas, VA) cells were maintained as subconfluent cultures by passage every 3 d from cultures seeded at 5000 cells/cm^2 in 8% calf serum/DMEM. For differentiation assays, cells were seeded at 15×10^3 cells per well into 24-well tissue culture plates in 8% fetal bovine serum/DMEM, after which cultures were grown for 2 d and then treated with the indicated RXR, RAR, and PPAR ligands either with or without MDIT (100 μM 3-isobutyl-1-methylxanthine, 100 nM dexamethasone, 0.1 ng/ml insulin, and 2 nM T_3 thyroid hormone) induction cocktail. Media and ligand treatments were renewed every 2 d. After 1 wk, cells were scored for adipocyte differentiation by Oil Red O staining for lipid droplet accumulation. Cultures were washed with PBS, fixed with 10% formaldehyde for 15 min, washed with distilled water, and stained with filtered Oil Red O solution (4 g/liter, 60% isopropanol) for 15 min. Excess stain was removed by washing three times with distilled water. Three random fields from each well were photographed under phase contrast and analyzed in ImageJ. Images were converted into high-contrast black and white images to visualize lipid droplets and scored as the percentage area per field. Data are shown as the mean ± SEM from three wells per treatment. The method was validated by extraction of Oil Red O from stained cells into 100% isopropanol and quantitated by absorbance at 540 nm on a spectrophotometer.

In Vivo Animal Exposure Experiments

C57BL/6J mice were housed under a 12-h light, 12-h dark cycle. Pregnant mice were dosed by ip injection with TBT [0.05 or 0.5 mg/kg body weight (b.w.)] or vehicle (sesame oil) from embryonic d 12 (E12) every 24 h until the day before delivery. Neonates were killed at the day of delivery and analyzed. The samples were embedded in optimal cutting temperature embedding compound and sectioned (12 mm) using a cryostat. Sections were fixed on slides with 4% paraformaldehyde for 10 min and rinsed in PBS. The slides were then sequentially washed with distilled water and 60% of isopropanol and stained with Oil Red O (4 g/liter, 60% isopropanol). After washing with 60% isopropanol and distilled water, the slides were counterstained with hematoxylin. Sections were evaluated and photographed using a Zeiss microscope (Carl Zeiss, Thornwood, NY).

For long-term growth studies, pups were cross-fostered to unexposed C57BL/6 dams after birth, and litter sizes were kept constant at eight pups per dam (control, two male + two female; TBT treated, two male + two female). Animals were weaned at 3 wk of age and maintained on standard rodent chow. Total body weight was followed until 10 wk of age. Males were then killed, and epididymal fat pads were dissected and weighed.

X. laevis tadpoles were sorted at stage 48 (89) and maintained in 1-liter glass tanks in 20% Holtfreter's buffered salt solution (90) at a density of 10 tadpoles per tank on a diet of ground Tetramin Fish Flakes and spirulina. Compounds prepared in dimethylsulfoxide (DMSO) as 10^5-fold stock solutions were tested on triplicate tanks and dosed by static renewal after weekly water changes. Metamorphs at stage 64 were transferred to individual containers and fed frozen brine shrimp for 2 wk until stage 66. Froglets were euthanized with 250 mg/liter MS222 in 20% Holtfreter's solution and then scored for gonadal abnormalities and interrenal/gonadal adipocyte formation under a dissecting microscope. Kidneys with attached gonads and livers were fixed in 10% formalin-PBS, embedded in paraffin, and sectioned at 15 μm thickness. Sections were developed with Mallory's trichrome stain.

All animal experiments were approved and performed in accordance with Institutional Animal Care and Use Committee protocols.

Acknowledgments

We thank Drs. I. Blitz, K. Cho, C. Zhou, and T. Osborne for critical reading and comments on the manuscript, Dr. C. Li (Expression Technologies) for the H_6-RXRα LBD construct, and Dr. R. Chandraratna (Allergan Pharmaceuticals, Irvine, CA) for AGN203 and LG268).

Received September 8, 2005. Accepted March 30, 2006.

Address all correspondence and requests for reprints to: Bruce Blumberg, Department of Developmental and Cell Biology, University of California Irvine, 2113 McGaugh Hall, Irvine, California 92697-2300. E-mail: blumberg@uci.edu.

This work was supported by grants from the U.S. Environmental Protection Agency (STAR R830686) and National Institutes of Health (GM-60572) (to B.B.); from the Ministries of Education, Culture, Sports, Science and Technology, Environment and Health Labor and Welfare, Japan (to T.I.); and from the University of California Toxic Substance Research and Training Program (UC-37579) (to F.G.).

F.G., H.W., Z.Z., L.M., K.A., R.C., D.M.G., J.K., T.I. have nothing to declare. B.B. is a named inventor on U.S. patents US 5,861,274, US 6,200,802, and US 6,815,168.

REFERENCES

1. Appel KE 2004 Organotin compounds: toxicokinetic aspects. Drug Metab Rev 36:763–786
2. Golub M, Doherty J 2004 Triphenyltin as a potential human endocrine disruptor. J Toxicol Environ Health B Crit Rev 7:281–295
3. Blaber SJM 1970 The occurrence of a penis-like outgrowth behind the right tentacle in spent females of *Nucella lapillus*. Proc Malacolog Soc London 39:231–233
4. Gibbs P, Bryan G 1986 Reproductive failure in populations of the dog-whelk, *Nucella lapillus*, caused by imposex induced by tributyltin from antifouling paints. J Mar Biol Assoc UK 66:767–777
5. Matthiessen P, Gibbs P 1998 Critical appraisal of the evidence for tributyltin-mediated endocrine disruption in mollusks. Environ Toxicol Chem 17:37–43
6. Shimasaki Y, Kitano T, Oshima Y, Inoue S, Imada N, Honjo T 2003 Tributyltin causes masculinization in fish. Environ Toxicol Chem 22:141–144
7. McAllister BG, Kime DE 2003 Early life exposure to environmental levels of the aromatase inhibitor tributyltin causes masculinisation and irreversible sperm damage in zebrafish (*Danio rerio*). Aquat Toxicol 65:309–316
8. Omura M, Ogata R, Kubo K, Shimasaki Y, Aou S, Oshima Y, Tanaka A, Hirata M, Makita Y, Inoue N 2001 Two-generation reproductive toxicity study of tributyltin chloride in male rats. Toxicol Sci 64:224–232
9. Ogata R, Omura M, Shimasaki Y, Kubo K, Oshima Y, Aou S, Inoue N 2001 Two-generation reproductive toxicity